Manuscript submitted to Tectonics: Peer review pending.

Post-collisional reorganisation of the Eastern Alps in 4D: Crust and mantle structure

Peter J. McPhee[1] and Mark R. Handy[1, 2]

1. Institute of Geological Sciences, Freie Universität Berlin, Germany (peter.mcphee@fu-berlin.de)
2. Institute of Geological Sciences, Universität Bern, Switzerland

Abstract

The Eastern Alps were affected by a profound post-collisional tectonic reorganisation in Neogene time, featuring indentation by the Adriatic upper plate, rapid uplift and filling of the eastern Molasse Basin, rapid exhumation and eastward orogen-parallel transport of Tertiary metamorphic units in the orogenic core, and a shift from northward thrust propagation in the European plate to southward propagation in the Adriatic plate. We test the idea that these events were triggered by slab detachment by reconstructing the indentation process. This involved sequentially restoring N-S and E-W cross-sections of the orogenic wedge and correcting for out-of-section orogen-parallel transport with a map-view reconstruction. We propose two phases of indentation: Initially (23-14 Ma), the whole Adriatic crust acted as an indenter. Its northward motion was accommodated by upright folding and orogen-parallel extensional exhumation in the Tauern Window. This phase was followed (14 Ma-Present) by continued orogen-parallel transport of the orogenic edifice into the Pannonian Basin and deformation of the leading edge of the Adriatic indenter, forming the Southern Alps fold-thrust belt. The lower crust of the Southern Alps indented the base of the Venediger Nappes in the Tauern Window, forming a high-velocity (6.8-7.25 km/s) ridge at 30-45 km depth in map view. By correlating the post-23 Ma orogenic evolution with presently imaged European slab segments in P-wave teleseismic tomography, we discern two possible Neogene slab detachment events: One at 23-19 Ma triggering tectonic reorganisation of the Eastern Alps and its foreland basin, and potentially a second event after 14 Ma.

Keywords:

Indentation and extrusion tectonics; European Alps; lower crustal wedging; slab detachment

Highlights:

- The Eastern Alps were first indented by Adriatic lithosphere (23-14 Ma), then by Adriatic lower crust as the indenter deformed (14-0 Ma).
- Shortening of the orogenic wedge since 23 Ma requires 135 km of subduction and 90 km of eastward extrusion of orogenic lithosphere.
- Slab detachment at 23-20 Ma and possibly after 14 Ma is constrained by areal balancing of crust and mantle.

1. Introduction

Slab detachment, also known as break-off, is a commonly invoked process affecting the post-collisional evolution of orogenic belts. In this paper, we sometimes use the term *slab removal* as a more neutral, non-mechanistic term to describe the elimination of subducted lithosphere from beneath orogens. By whatever means, releasing the slab-pull force is predicted to drive uplift (e.g., Buiter et al., 2002; Duretz et al., 2011), shaping orogens and their peripheral basins (e.g., Fox et al., 2015; Sinclair, 1997). Slab remnants that have detached and sunk into the mantle have been widely imaged in seismic tomography, particularly below orogenic belts (e.g., Van Der Meer et al., 2018; Wortel & Spakman, 2000). Yet, discerning the geological signals of slab detachment above these remnants, particularly uplift, is challenging because orogenic processes such as crustal shortening may conceal them. Additionally, a scarcity of high-resolution geophysical data and an incomplete picture of orogenic evolution often complicates detailed examination of the relationship between subduction, orogenesis, and slab detachment. Together, these uncertainties have driven much discussion and controversy surrounding the role of slab detachment in shaping collision in the Alps and beyond (e.g., Garzanti et al., 2018; Kästle et al., 2020).

Recently, the Eastern Alpine crust and mantle have been seismologically imaged in unprecedented detail using a network of over 600 temporary broadband stations deployed during the *AlpArray* passive array experiment (2015-2019, AlpArray Seismic Network Team et al., 2018; average station spacing of 40 km), as well as an even denser targeted array of 163 stations over the Eastern and eastern Southern Alps (Swath D, average station spacing of 15 km, Heit et al., 2023). P-wave teleseismic models reveal high-velocity anomalies interpreted as subducted and partly detached slabs (Handy et al., 2021; Paffrath et al., 2021). In contrast to classical ideas of subduction in collisional settings that involve horizontally continuous slabs and single detachment events (e.g., von Blanckenburg & Davies 1995), positive slab anomalies below the Eastern Alps have a non-cylindrical structure with vertical and horizontal gaps (e.g., Handy et al., 2021; Malusà et al., 2021). If this AlpArray-derived teleseismic model represents the mantle structure accurately, it may demonstrate a complex history of orogen-parallel slab segmentation, potentially with more than one slab removal event.

Unlike the Western and Central Alps, north directed orogenesis in the Eastern Alps was significantly modified by orogen-parallel transport of the orogenic edifice in Neogene times (e.g., Frisch et al., 2000; Ratschbacher et al., 1991, Schmid et al. 2013). Those events broadly coincided with a switch in orogenic polarity from N-directed thrusting in the Eastern Alps to S-directed thrusting in the

Southern Alps (Handy et al. 2023), as well as sudden infilling and uplift of the eastern Molasse Basin (Genser et al. 2007, Le Breton et al. 2023).

We define the Eastern Alps as the tectonic units east of the Brenner Fault and north of the Giudicarie and Periadriatic Faults (Fig. 1, hatched area bounded by lines labelled BF, GF, and PF). This is important from the standpoint of Neogene tectonics and differs from the broader, more generally used definition of Eastern Alps as the far-travelled Austroalpine Nappes overlying the Paleogene nappe stack in the Alps (Schmid et al., 2004, coloured purple in Fig. 1).

Here, we examine the relationship between mantle and crustal structure in the Eastern Alps during its Neogene tectonic reorganisation. This is crucial for understanding the role of slab removal in shaping the Eastern Alps. After a brief introduction to the geology of the Eastern Alps (Chapter 2), we summarize recently published local earthquake tomography (LET) to shed new light on the structure of the lower and intermediate crust beneath the Eastern Alps (Chapter 3). We reconstruct the structure of the crust and mantle (Chapter 4) by restoring Neogene deformation along two orogen-normal cross-sections (Chapter 5) – the well-known TRANSALP transect at ~12°E (e.g., Lüschen et al., 2004) that employed controlled-source seismology (CSS), and the *Eastern Alpine Seismological Initiative* (EASI) transect at 13.3°E (e.g., Hetényi et al., 2018) based on a passive-array swath experiment conducted in an early stage of the *AlpArray* project. In addition, we present an E-W orogen-parallel cross-section that intersects the TRANSALP and EASI transects (Fig. 2). To make the balancing of Neogene tectonics truly three-dimensional, the effects of eastward orogen-parallel transport in the N-S cross-sections are accounted for using a map-view reconstruction (Chapter 5). We then integrate these results with local earthquake tomography (LET) to investigate the structural style and fate of the lower crust and lithospheric mantle during the switch from north- to south-directed thrusting across the orogen (Chapter 6). Finally, in Chapter 7, we integrate the new seismological and geological data along the balanced cross sections to constrain the timing and kinematics of indentation, as well as to infer the mechanical response of both indented and indenting crustal during slab removal. It is argued that one, possibly two, Neogene slab removal events involving different mechanisms affected the Eastern Alps.

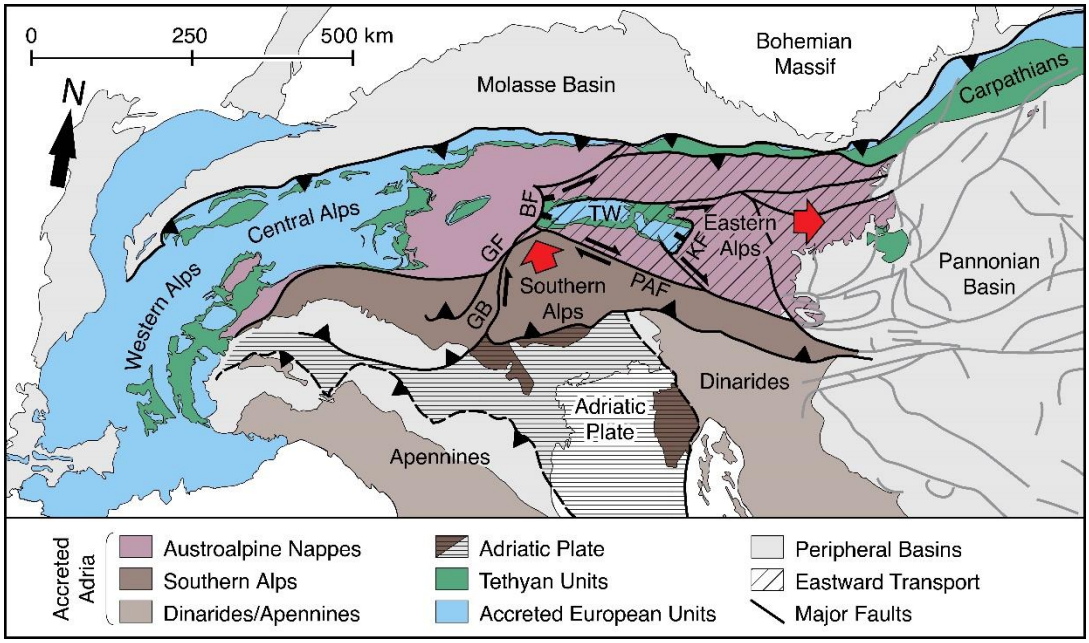

Figure 1: Tectonic map of the Alps and surrounding basins and mountain belts (redrawn after Handy et al., 2019, and Schmid et al., 2004). BF – Brenner Fault; GB – Giudicarie Belt; GF – Giudicarie Fault; KF – Katschberg Fault; PAF – Periadriatic Fault; TW – Tauern Window.

2. Geological setting

The Eastern Alps comprise rocks derived from the subducted European continent (Tauern Window), the Adriatic continental upper plate (Austroalpine Nappes and Southern Alps), and the accreted remains of the Mesozoic Alpine Tethyan Ocean (Alpine Tethys) that once separated these continents (Fig. 1). Subduction of the Alpine Tethys in Late Cretaceous time was followed by the Adria-Europe continental collision in the late Eocene, marked by the incorporation of distal European passive margin units into the orogenic wedge and deposition of orogen-derived sediments on the European foreland. We start by outlining the tectonic units in our cross-sections, following the subdivision of Schmid et al. (2004).

The eastern Molasse Basin is the northern foreland basin of the Eastern Alps and records erosion of the Alpine orogen during its northward advance with respect to Europe. Initial deposition from 33-28 Ma was followed by the development of a basin-wide unconformity, the Northern Slope Unconformity or NSU, which records the over-steepening of the basin floor (Masalimova et al., 2015). The eastern Molasse Basin experienced deep marine deposition from ~25-19 Ma, followed by rapid infilling and tectonic uplift at around 19-17 Ma (e.g., Hülscher et al., 2019; Kuhlemann & Kempf, 2002). The Subalpine Molasse comprises folded and thrusted slices of the Molasse Basin and is the northernmost and structurally lowest tectonic unit on the northern side of the Eastern Alps

(e.g., Ortner et al., 2011, 2022). In the Eastern Alps, thrusting of the Subalpine Molasse advanced northward until early Miocene time, when the thrusts were sealed by lower Miocene (Aquitanian-Burdigalian, 23-20 Ma) strata in the western part of the eastern Molasse Basin (i.e., west of Salzburg, Fig. 2; Hinsch, 2013). After that, only minor out-of-sequence deformation affected the northern orogenic front and thrusting stepped back into the orogen.

The Helvetic Nappes, structurally above the Subalpine Molasse, comprise Permo-Mesozoic sedimentary rocks derived from the former European passive margin of Alpine Tethys (e.g., Pfiffner, 1993). These nappes are poorly exposed along the Eastern Alpine orogenic front and are intercalated with equally poorly exposed thrust slices of the structurally higher Penninic Nappes. The Penninic Nappes consist of marine sedimentary and ophiolitic rocks derived from the subducted Alpine Tethys (e.g., Kurz et al., 1996; Schmid et al., 2004). In the Tauern Window, where the Penninic Nappes are best exposed, they record Paleogene high-pressure (HP) and subsequent high-temperature (HT) metamorphism (e.g., Hoinkes et al., 1999; Schuster et al., 2004).

The Austroalpine Nappes are the structurally highest nappes in the Alps and are derived from the southern passive margin of the Adriatic continent. Nappe stacking occurred during the Cretaceous Eoalpine Orogeny. During subsequent subduction of the Alpine Tethyan Ocean and Adria-Europe collision, this older nappe stack formed a rigid upper plate (e.g., Handy et al., 2010). Across the Eastern Alps, the Austroalpine Nappes are unconformably overlain by outliers of the Late Cretaceous to Paleogene syn- to post-orogenic marine Gosau Basins (e.g., Wagreich & Faupl, 1994).

On the northern side of the Eastern Alps, the Austroalpine Nappes include the far-travelled North Calcareous Alps, comprising the weakly- to non-metamorphic Juvavic, Tirolean, and Bavarian nappes (Fig. 1) that were accreted in Cretaceous time from the northern margin of the Neotethyan ocean (Frisch & Gawlick, 2003; Schmid et al., 2004). These contain a Permian to Cretaceous carbonate-dominated sequence of sedimentary rocks, plus the Palaeozoic Grauwackenzone of the Tirolean Nappe. The structurally underlying Austroalpine Basement Nappes are best exposed to the south of the North Calcareous Alps and comprise basement and cover that experienced Late Cretaceous high-temperature and high-pressure metamorphism during the Eoalpine orogeny (e.g., Hoinkes et al., 1999; Schuster et al., 2004).

The Tauern Window exposes subducted, accreted, and metamorphosed units of the European passive margin (Venediger Nappes) and overlying Penninic Nappes. The Venediger Nappes comprise a thrust duplex of European basement slices separated by thinned Permo-Mesozoic cover rocks (e.g., Groß et al., 2020, 2022). These underwent high-pressure metamorphism in Paleogene time (e.g., Handy & Oberhänsli, 2004; Liu et al., 2001) before the entire thrust duplex was overprinted by

high-temperature, Barrovian-type metamorphism at peak conditions of 620°C, 0.7 GPa at 28-30 Ma (e.g., Favaro et al., 2015).

The Tauern Window (Fig. 2) is bounded to the W and E by oppositely dipping, low-angle normal faults (Brenner and Katschberg faults, respectively) and to the N and S by conjugate strike-slip faults. Together, these faults accommodated E-W extension and E-directed orogen-parallel motion of the Eastern Alpine orogenic crust (Fig. 1; e.g., Linzer et al., 2002; Ratschbacher et al. 1989, 1991; Frisch, et al., 1991). Our cross-sections (Fig. 4, traces in Fig. 2) transect these strike-slip faults.

Cooling of the Venediger Nappes began in the Oligo-Miocene (~28-23 Ma) and accelerated in early to middle Miocene time (~23-9 Ma, e.g., Favaro et al., 2015; Fügenschuh et al., 1997; Luth & Willingshofer, 2008; Rudmann et al., 2024). This cooling has been attributed to exhumation involving a combination of broadly coeval upright post-nappe folding, erosion, and extensional exhumation in the footwalls of the Brenner and Katschberg normal faults (Bertrand et al., 2017; Favaro et al., 2017; Rosenberg et al., 2018; Scharf et al., 2013).

The Southern Alpine fold-thrust belt located south of the Periadriatic Fault comprises non-metamorphic Permo-Mesozoic cover and basement derived from the Adriatic margin that was adjacent to Alpine Tethyan Ocean (e.g., Bertotti et al., 1993; Winterer & Bosellini, 1981). Unlike the Austroalpine Nappes, the Southern Alps are not far-travelled and feature (W)SW and S-directed thrusting. The eastern Southern Alps are separated from the central and western parts of the Southern Alps by the Giudicarie Belt (Fig. 1), an oblique sinistral transpressional fold-thrust belt (e.g., Picotti et al., 1995; Verwater et al., 2021) which, together with the NNE-SSW-trending Giudicarie Fault, was active in early-to-late Miocene time (Pomella et al., 2011, 2012). The Giudicarie Belt sinistrally offsets the Periadriatic Fault and Oligocene Periadriatic intrusive rocks (marked red in Fig. 2), subdividing the Adriatic indenter into the Ivrea (western) and Dolomites (eastern) subindenters (e.g., Handy et al., 2015; Rosenberg et al., 2015). In the eastern Southern Alps, thrust faults rooting in the basement formed since middle Miocene times, as dated by the occurrence of lower-to-middle Miocene sedimentary rocks in their footwalls (Castellarin et al. 1998, Verwater et al., 2021, and references therein). This age is corroborated by the flexural deepening of the Veneto-Friuli Basin (Mellere et al., 2000) and by thermal modelling of cooling ages along eroded hangingwall anticlines above thrust faults (Eizenhöfer et al., 2023). The thrusts in the easternmost Southern Alps offset older SW-directed thin-skinned thrusts of the Late Cretaceous-to Paleogene Dinaric fold-thrust belt (e.g., Merlini et al., 2002; Poli & Zanferrari, 2018; Ponton, 2010). West of the Giudicarie Belt, Miocene thrusting affecting the basement was preceded by an earlier phase (Late Cretaceous or

Paleogene?) of thrusts crosscut by the Oligocene Adamello intrusion (e.g., Brack, 1981; Schönborn, 1992).

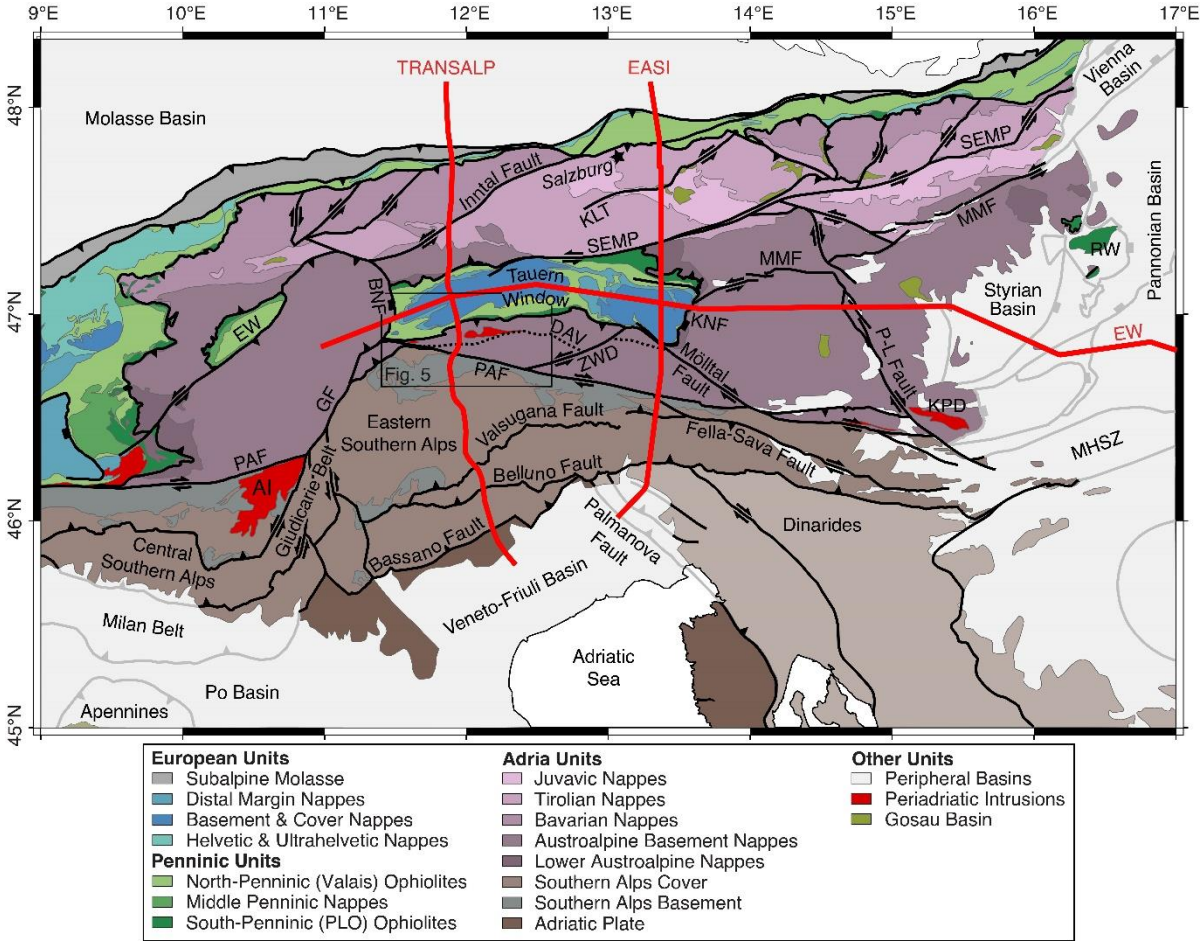

Figure 2: Tectonic map of the Central and Eastern Alps based on Schmid et al. (2004) and faults from McPhee et al. (in prep). Thick red lines indicate traces of the TRANSALP, EASI, and EW cross-sections in this study. Abbreviations: AI – Adamello Intrusion; DAV – Defereggen-Anterselva/Antholz-Valles/Vals Fault; BF – Brenner Fault; EW – Engadin Window; GF – Giudicarie Fault; KLT – Königsee-Lammertal-Traunsee Fault; KF – Katschberg Fault; KPD – Kozak and Pohorje Domes; MHSZ – Mid Hungarian Shear Zone; MMF – Mur-Mürz Fault; PAF – Periadriatic Fault; P-L – Pols-Lavanttal; RW – Rechnitz Window; SEMP – Salzach-Ennstal-Mariazell-Puchberg Fault; ZWD – Zwischenbergen-Wollatratten-Drau Fault.

3. Tomographic models of the Eastern and Southern Alps

High-quality data from a dense network of temporary stations of the AlpArray and SWATH-D experiments allows us to use local earthquake tomography (LET) to visualise the P-wave velocity structure down to 60 km depth at a node spacing of 5-15 km (Jozi Najafabadi et al. 2022). P-wave

velocities reflect the bulk physical properties of rock averaged over a volume roughly proportional to the spacing between seismic stations at the surface. Although LET is a truly 3D method that yields potentially high-resolution and reliable 3D velocity information for consistent datasets, LET models do not directly reproduce velocity discontinuities such as the Moho or crustal-scale faults, instead resolving these as smooth velocity gradients.

In the LET model of Jozi Najafabadi et al. (2022), the Moho in Figure 3A is defined by a proxy velocity value of 7.25 km/s, an average of lower crustal and upper mantle velocities. For comparison, Figure 3B shows the Moho map of Spada et al. (2013) based on a weighted combination of Moho depth estimates from LET, Receiver Function (RF), and controlled-source seismic (CSS) methods. The white area in Figure 3B indicates where no Moho could be imaged due to a very low velocity gradient (0.08 s^{-1}, Diehl et al. 2009). Thus, we define the Moho in our cross-sections in Figure 4 as the mean trace of available Moho models along each geophysical transect (LET – Jozi Najafabadi et al., 2022; Diehl et al., 2009; RF – Bianchi et al., 2021; Hetényi et al., 2018; Kummerow et al., 2004; Mroczek et al., 2023; joint inversion of LET, RF and CSS– Spada et al., 2013).

The boundary between lower and intermediate crust is taken to be a proxy velocity of 6.8 km/s (Fig. 3C), corresponding to an average of P-wave velocities measured in the laboratory on exhumed crustal rocks from the Ivrea-Verbano Zone in the western-most Southern Alps (Fig. 1; Burke & Fountain, 1990). There, a complete section of the Southern Alpine (Adriatic) crust is exposed, from non-metamorphic Permo-Mesozoic sedimentary rocks in the southeast to intermediate crustal, lower crustal and upper mantle rocks in the northwest (Zingg et al., 1990). The rocks in the Ivrea section are typical of both the Adriatic and European lower crust because they share a common late Paleozoic and Early Mesozoic history before the opening of Alpine Tethys (e.g., Handy et al., 1999).

To determine the thickness of the lower crust, we subtracted the depths of the 6.8 km/s (Fig. 3C) and 7.25 km/s isovelocity surfaces (Fig. 3A) and the Moho model of Spada et al. (2013) (Fig. 3B). The resulting thickness maps (Figs. 3D and 3E) show that in the Central Alps west of the Giudicarie Fault, the lower crust is thickened north of the Periadriatic Fault. East of the Giudicarie Fault, a thick ridge of lower crusts runs subparallel to the Giudicarie Fault beneath the Southern Alps, then extends northward to beneath the SW corner of the Tauern Window, where it attains its greatest thickness. The Moho is not offset by the Giudicarie Belt and Line (Figs. 3A, B), suggesting this major fault system is confined to the crust. In the eastern Southern Alps, the 6.8 km/s isovelocity surface deepens from the Veneto-Friuli Basin towards the Periadriatic Fault (Fig. 3C). North of the Periadriatic Fault and beneath the Tauern Window, the 6.8 km/s isovelocity surface shallows to the north and east.

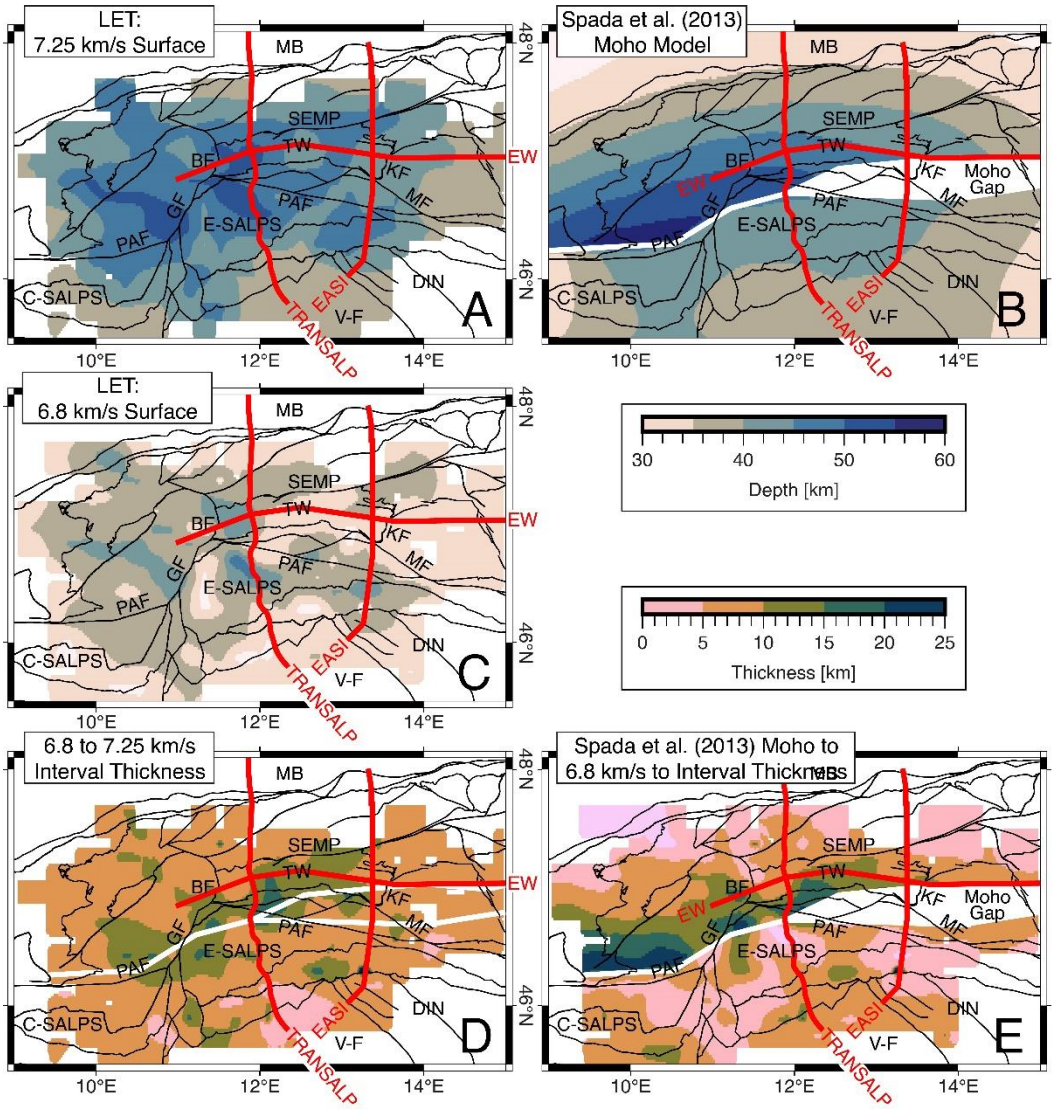

Figure 3: LET data across the Eastern Alps, with black lines defining major thrusts and strike-slip faults. Abbreviations: BF – Brenner Fault; DIN – Dinarides; KF – Katschberg Fault; MB – Molasse Basin; GF – Giudicarie Fault; PAF – Periadriatic Fault; C-SALPS – central Southern Alps; E-SALPS – eastern Southern Alps; SEMP – Salzach-Ennstal-Mariazell-Puchberg Fault; TW – Tauern Window; V-F – Veneto-Friuli Basin (See Figure 2 for additional labels). (**A)** 7.25 km/s (Moho proxy) isovelocity surfaces from Jozi-Najafabadi et al. (2022). (**B)** Spada et al. (2013) Moho model. (**C)** 6.8 km/s (top lower crust proxy) isovelocity surfaces from (Jozi Najafabadi et al. (2022). (**D)** 7.25 to 6.8 km/s interval thickness, interpreted to represent lower crustal thickness. (**E)** 6.8 km/s (top lower crust proxy) isovelocity surface to Spada et al. (2013) Moho model.

4. Section construction and reconstruction approach

We constructed our cross-sections in the structural modelling and analysis software *Move*™ 2019, assuming minimum shortening. Where available, we used and adapted existing subsurface interpretations. We linked structures exposed at the surface to the LET and Moho models in the subsurface. Along the TRANSALP cross-section, we used reflectors manually picked from vibroseis- and dynamite-source seismic data and presented in Lüschen et al. (2006).

In the Neogene, the Eastern Alps were transected by dextral and sinistral strike-slip faults that facilitated eastward orogen-parallel transport of the orogenic wedge (Figs. 1 and 2; e.g., Favaro et al., 2017; Linzer et al., 2002; Ratschbacher, Frisch, et al., 1991; Rosenberg et al., 2018). In our north-south-orientated cross-sections, this transport violates a basic assumption of plane strain made in 2D balancing (i.e., motion only in the plane of the cross-section). To address this, we utilised a map-view reconstruction (McPhee et al., in prep) to restore out-of-section transport at 23 and 14 Ma. These periods were chosen to represent the initiation of accelerated cooling of the Venediger Nappes, related to extension and upright folding (23 Ma) and the initiation of south-directed thrusting in the eastern Southern Alps (14 Ma). We first retrodeformed the map-view reconstruction to the timesteps of interest, drawing straight cross-section traces that connected the EASI and TRANSALP cross-sections from the European foreland to the Southern Alps. We then forward-modelled the map-view reconstruction, translating segments of the 14 and 23 Ma cross-sections to their present locations (coloured segments in Fig. 4). Finally, we interpreted the present structure in the offset section traces. We assembled them into composite cross-sections representing the orogen at 14 and 23 Ma. Our composite sections maintain the present-day cross-sectional area of the accreted European units exposed in the Tauern Window.

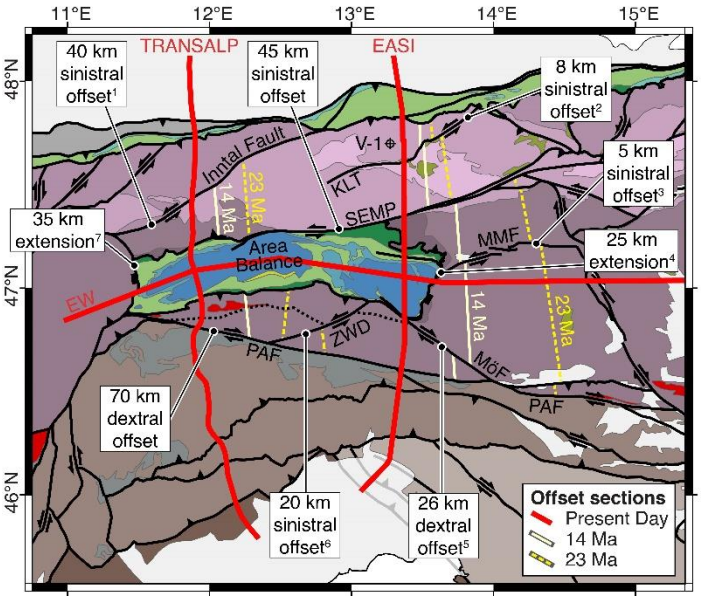

Figure 4: Part of Figure 2 showing the offset cross-sections used to correct for the effects of eastward orogen-parallel transport. These were located using the a map-view reconstruction based on total strike-slip offset estimates from: (1) Inntal Fault – Ortner et al. (2006); (2) KLT – Königsee-Lammertal-Traunsee – Linzer et al. (2002); (3) MMF – Mur-Mürz Fault – Eder & Neubauer (2000); (4) KF – Katschberg Fault – Scharf et al., 2013; (5) MöF – Mölltal Fault (Favaro et al., 2017); (6) ZWD – Zwischenbergen-Wollatratten-Drau Fault – Favaro et al. (2017); (7) BF – Brenner Fault – Wolff et al. (2021). Estimated Neogene offset along the Salzach-Ennstal-Mariazell-Puchberg Fault (SEMP) and Periadriatic Fault (PAF) offsets are resulting from these constraints. V-1 is the location of the Vorderriss-1 borehole (Bachmann & Müller, 1981). See Figure 2 for the legend.

5. Present structure

Figure 5 shows the present orogenic structure of the Eastern Alps in three cross-sections that depict key structural features. These sections form the basis of the retrodeformation in the next chapter, where we demonstrate that our cross-sections are balanced and kinematically viable.

TRANSALP

Along the TRANSALP cross-section (TRANSALP Working Group, 2002), the segment between the Molasse Basin and the DAV fault (Fig. 2) is based on existing structural interpretations across the Subalpine Molasse and Penninic and Helvetic nappes (Ortner et al. 2014), the North Calcareous Alps to the Inntal Fault (Auer & Eisbacher 2003) and between the Inntal Fault and Tauern Window (Ortner et al. 2006). A package of seismic reflectors dips gently southward from the foreland, marking the Penninic and Helvetic nappes and Permo-Mesozoic cover of the European crust below

the North Calcareous Alps (Fig. 6A). Following previous interpretations (e.g., Lüschen et al., 2006), we link these reflectors to the Adriatic Moho along a ramp beneath the Tauern Window, the *Sub-Tauern Ramp*. This major thrust runs parallel to south-dipping seismic reflectors at the base of the Venediger Nappes. Receiver function models of the Moho along the TRANSALP cross-section (Kummerow et al., 2004; Mroczek et al., 2023) show that the European Moho dips south beneath the Adriatic Moho and is separated from the latter by a vertical gap. We interpret this gap to represent subducted European crust, corresponding to a positive anomaly in the local earthquake (Fig. 6A; Jozi Najafabadi et al. 2022) and teleseismic P-wave tomographic images (Fig. 7A; Handy et al., 2021; Paffrath et al., 2021).

Following the near-surface structural interpretation of Schmid et al. (2013; their Section 3) across the Tauern Window to the DAV, we link the Penninic Nappes at the surface to moderately south-dipping seismic reflectors at 14-18 km depth (e.g., TRANSALP Working Group et al., 2002). This package of reflectors is sub-parallel to reflectivity in the adjacent Austroalpine Nappes and Southern Alpine basement and terminates abruptly down-dip, leading us to interpret a fault offset that we link vertically upwards to the surface trace of the Periadriatic Fault (marked PAF in Fig. 6A). We interpret the Venediger, Penninic, and Austroalpine nappes as continuing southwards at depth, forming a south-tapering wedge of intermediate crust below the Southern Alps (Fig. 6A).

Our interpretation of the Periadriatic Fault in the TRANSALP section is consistent with observations at the surface that this fault is a brittle structure that obliquely cuts the folded contacts between the Austroalpine, Penninic, and Venediger nappes, and also truncates the Neogene cooling age contours (Fig. 5) at the southwest corner of the Tauern Window (Handy et al., 2005; Luth & Willingshofer 2008). Slip along this fault was right-lateral with only a few kilometres of north-side up motion during the late Oligocene and Miocene (Luth & Willingshofer, 2008; Mancktelow et al., 2001; Ratschbacher et al., 1991). The Periadriatic Fault, therefore, post-dates not only nappe formation but also most of the exhumation of these nappes in Tertiary time. The main foliation parallel to the steeply S-dipping nappe contacts cut by the Periadriatic Fault accommodated the bulk of shearing related to nappe exhumation since 30 Ma (≤ 25 km, Handy et al. 2005, their Fig. 5 and references therein). In Figure 6A, this foliation is interpreted to correspond to the S-dipping reflectors that continue at depth to the south beneath the Southern Alps.

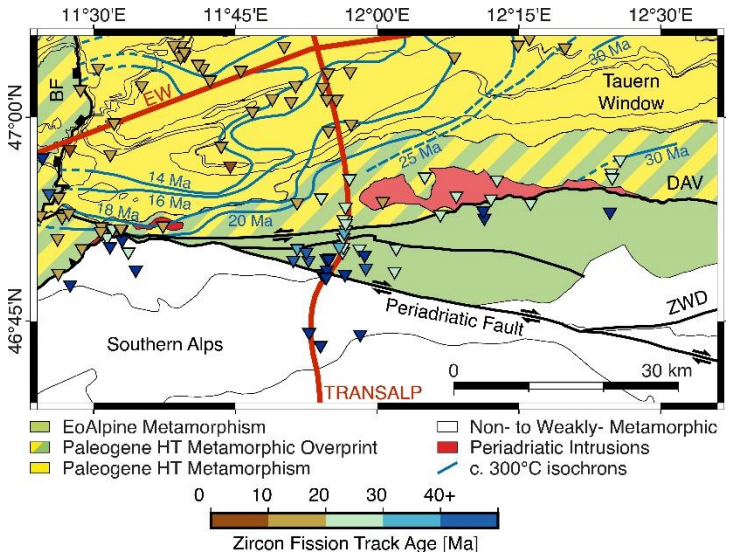

Figure 5: Map of the southwestern Tauern Window showing where the Periadriatic Fault cuts the S-dipping Paleogene nappe contacts (taken here from Schmid et al. 2013) as well as Paleogene high temperature (HT) metamorphism (Schuster et al., 2004) and Neogene isochrons related to post-nappe cooling and exhumation. Blue contours are 300°C cooling isochrons from Handy & Oberhänsli (2004), based on a compilation of biotite Rb-Sr and Ar-Ar white mica cooling ages. Zircon fission track ages compiled from Bertrand et al., (2017); Elias, (1998); Fügenschuh, (1995); Klotz et al., (2019); Most, (2003); Pomella et al., (2012); Steenken et al., (2002); Stöckhert et al., (1999); Viola et al. (2001). BF – Brenner Fault; DAV – Defereggen-Anterselva/Antholz-Valles/Vals Fault; ZWD – Zwischenbergen-Wollatratten-Drau Fault.

Our interpretation of the deep structure of the TRANSALP section (Fig. 6A) differs from interpretations of the TRANSALP Working Group (2002) in which the contacts between the Venediger, Penninic, and Austroalpine Nappes, as well as the Periadriatic fault at the surface were extrapolated to depth in very different ways: (1) S-dipping and concordant with the south-dipping reflectors (their Model A) and; (2) steeply to N-dipping and discordant with these reflectors (their Model B, see also Castellarin et al. 2006b). In the second scenario, the Periadriatic Fault was inferred to connect northward with the Sub-Tauern Ramp at depth to accommodate vertical exhumation and eastward lateral escape of the metamorphic core that comprises the Eastern Alps in the Tauern Window. Interpretations since then have adopted variants of these two end-member models (e.g., Schmid et al. 2004, 2013; Rosenberg et al. 2018), with most authors adopting variations of the TRANSALP B "lateral extrusion" model. Unfortunately, the deep structure of the Periadriatic Fault remains virtually unconstrained despite repeated efforts to address the challenge of imaging discrete subvertical structures with low impendence contrasts (e.g., 3D-Kirckhoff stack migration, Bleibinhaus & Groschup, 2008; Seismic diffraction imaging, Bauer et al., 2024). A subvertical Periadriatic Fault that connects at depth with a detachment surface beneath the Tauern Window

(Fig. 6A) is consistent with the aforementioned field observations and satisfies the kinematic necessity of accommodating coeval N-S shortening and eastward lateral extrusion in Neogene time.

South of the Periadriatic Fault, we reconstructed the Southern Alpine fold-thrust belt using 1:50,000 and 1:100,000 geological maps published by the Geological Survey of Italy (see supplementary materials) and incorporating the structural interpretations of the Montello and Bassano anticlines Picotti et al. (2022) based on reprocessed seismic reflection, borehole, and surface geological data. The Southern Alps are deformed from north to south by the Valsugana Fault, Belluno Fault, Bassano Anticline, and Montello Anticline.

In the hangingwall of the Valsugana Fault, a thin-skinned fold-thrust belt deforms the Upper Permian to Cretaceous cover sequence of the Dolomites, with the evaporite-bearing Upper Permian Bellerophon Formation serving as a basal decollement. This formation is squeezed out along thrusts and in the cores of anticlines. We link part of this shortening to subsurface thrusts reaching into the basement. Most of the thrusts in the hangingwall of the Valsugana Fault are older SW-directed thrusts of the Dinaric fold-thrust belt (e.g., Castellarin & Cantelli, 2000; Doglioni & Bosellini, 1987).

The Dolomites are affected by open folds and an overall gentle north-dipping to subhorizontal regional dip (e.g., Castellarin et al., 1998). To reproduce this shallow regional dip above the stacked Valsugana, Belluno, Bassano, and Montello thrust faults, we found that the thick-skinned thrusts must link into a north-dipping ductile shear zone. This reaches down to 15–20 km depth, below the Bassano and Montello anticlines, and is associated with the deepest seismicity in the area (e.g., Anderlini et al., 2020). Such a ductile shear zone was previously proposed in balanced cross-sections (Nussbaum, 2000; Schönborn, 1999; Verwater et al., 2021) and thermo-kinematic models of the Southern Alps fold-thrust belt (Eizenhöfer et al., 2023).

As mentioned above, LET models of the Eastern Alpine crust consistently show an upward perturbation or bulge of velocity contours on the southern side of the Tauern Window (Diehl et al., 2009; Jozi Najafabadi et al., 2022). In map view, this bulge forms an E-W trending high-velocity structure some 5-10-km-high and oriented subparallel to the Eastern Alps just south of the Tauern Window (Fig. 3D). In the TRANSALP cross-section (Fig. 6A), this high-velocity bulge is located south of and below the Tauern Window, below the Periadriatic Fault and north of the Moho gap.

EASI

We use the cross-section of Hinsch (2013; their Fig. 8A) through the Subalpine Molasse, and Penninic and Helvetic nappes, which is based on borehole data and depth-migrated 3D seismic reflection

data. From the front of the North Calcareous Alps to the Periadriatic Fault, we construct the section in Figure 6B using 1:50,000 geological maps published by the Austrian Geological Survey (GeoSphere Austria; see supplementary materials) In the North Calcareous Alps, we incorporate the Vorderriss-1 borehole (Bachmann & Müller, 1981; Fig. 4), which penetrated the Tirolean Nappe and underlying Bavarian Nappe to reach the Penninic and Helvetic nappes. Analogous to the TRANSALP cross-section, we reconstruct these nappes above a south-dipping decollement as far south as the SEMP Fault (Fig. 2 and 6B). We assume that the regional dip of this thrust mimics that of the European Moho.

The SEMP sinistral strike-slip fault marks the southern limit of the North Calcareous Alps in the EASI section. It juxtaposes the lowest Austroalpine and underlying Penninic nappes with the structurally higher Tirolean Nappe (Fig. 6B). Between the SEMP and Tauern Window, folded Penninic rocks exposed to the west of the EASI cross-section (Fig. 2) lead us to interpret a thin cover of Austroalpine Basement rocks that plunge steeply south at the SEMP Fault to form a north-dipping monocline. We interpreted this monocline as the foreland-dipping limb of a fault-bend fold, marking the location of the subsurface Sub-Tauern Ramp. In contrast to the TRANSALP cross-section where the European and Adriatic Mohos are separated by a vertical gap (Fig. 6A), the Moho along the EASI cross-section is poorly defined in the vicinity of the Tauern Window and beneath the Periadriatic Fault, for the reasons pointed out above (Fig. 3B).

Our orogen-normal cross-section of the Venediger Nappes in the Tauern Window closely resembles those of Schmid et al. (2013) and Rosenberg et al. (2018). Figure 6B shows an open, upright fold in the Tauern Window with a vertical to overturned upper contact in the shallow subsurface that attains a shallower dip at depth.

The high-velocity bulge situated above the Moho gap, just south of the Tauern Window and below the Periadriatic Fault, decreases in amplitude going eastward from the TRANSALP to the EASI cross-sections (Figs. 3E, 6A, 6B). This may reflect a thinner lower crust and shallower Moho towards the east. We take the Moho gap to define the southern end of the European slab (e.g., Hetényi et al., 2018; Spada et al., 2013), which is directly underlain by a high-velocity anomaly in LET and teleseismic P-wave tomographic models, and then by a negative velocity anomaly in P-wave tomography (Handy et al., 2021; Paffrath et al., 2021).

To define the structure south of the Periadriatic Fault in the Southern Alps, we modify the cross-section of Ponton (2010), which incorporates seismic interpretations and borehole data of Merlini et al. (2002). Seismicity down to 15-20 km in the actively deforming, frontal part of the Southern Alps indicates that, as in the TRANSALP cross-section, thrusting is linked to shear zones deeply rooted in

the basement (e.g., Bressan et al., 2016). A NE-SW segment of this section allows balancing of orogen-normal shortening relative to the autochthonous Adriatic foreland. We extend the Ponton (2010) section north to the Periadriatic Fault based on the large-scale geological map of the Friuli-Venezia-Giulia region (Battista Carulli et al., 2006). There, we interpret a south-dipping monocline between the Periadriatic and Sava-Fella faults (marked PAF and S-F respectively, in Fig. 6B) where Palaeozoic sedimentary, volcanic, and basement rocks are exposed adjacent to the Periadriatic Fault. Our cross-section shows two major thrusts in the basement that splay upwards into the evaporite-bearing Upper Triassic Raibl Formation to form a thrust imbricate.

The EASI section includes the E-W striking Sava-Fella Fault (Fig. 2, marked S-F in Fig. 6B). A dextral offset of some 30 - 60 km has been proposed along the Slovenian segment of this fault based on a visual correlation of Oligocene volcanic rocks (e.g., Fodor et al., 1998). West of the EASI section (Fig. 2), this fault accommodates N-S shortening and subordinate dextral motion and terminates at a compressive horsetail structure (Bartel et al., 2014). Based on its hangingwall and footwall geometries, the Sava-Fella fault is reconstructed in Figure 6B as a subvertical south-dipping dextral-oblique thrust with minor associated fault splays (Jadoul & Nicora, 1986) that root in the basement (Merlini et al., 2002; Moulin & Benedetti, 2018; Nussbaum, 2000; Ponton, 2010).

Toward the foreland of the Southern Alps, Dinaric structures are unconformably covered by synorogenic sedimentary rocks of late Cretaceous to Paleogene age (Merlini et al., 2002) indicating that these structures were not significantly reactivated during Neogene deformation. North of the frontal thrusts, these sediments are absent, and so we rely on detailed structural analysis of Ponton (2010) to identify Dinaric thrust faults. Geological markers indicate a maximum of about 5 km of dextral offset across the system of Dinaric strike-slip faults (Moulin et al., 2016). This is consistent with estimates of up to 1 km from 1:50,000 scale geological map (Zanferrari et al., 2013) of associated fault splays. We modified the interpretation of Ponton (2010) to depict the Monte Simone Fault as a strike-slip fault (marked MS in Fig. 6B; Zanferrari et al., 2013), thereby removing an interpreted structural repetition of Mesozoic sedimentary rocks along a shallow-dipping Monte Simone Thrust (Merlini et al., 2002; Moulin & Benedetti, 2018).

EW (orogen-parallel)

In the E-W orogen-parallel section from the Central Alps to the Pannonian Basin (Fig. 6C), we use the Moho model of Spada et al. (2013), which closely matches the Moho proxy (7.25 km/s) in the LET model of Jozi Najafabadi et al. (2022). In the hangingwall of the Brenner Fault, we project west-plunging structures from the surface into the section and tie our interpretation to the NW-SE section

of Pomella et al. (2016; their Fig. 3B). Across the Tauern Window, we use a series of N-S and E-W oriented cross-sections from Schmid et al. (2013) and Groß et al. (2022) and augment our interpretation of the shallow-subsurface structure with structural information from tectonic contacts at the surface. In the hangingwall of the Katschberg Fault, we use 1:50,000 scale geological maps published by the Austrian Geological Survey (GeoSphere; see supplementary materials for details), projecting tectonic contacts down- or up-dip into the cross-section. Finally, in the Styrian and Pannonian Basins (shown only in Fig. 7C), we project the interpretation of the seismic reflection survey in Maros et al. (2012) onto our cross-section.

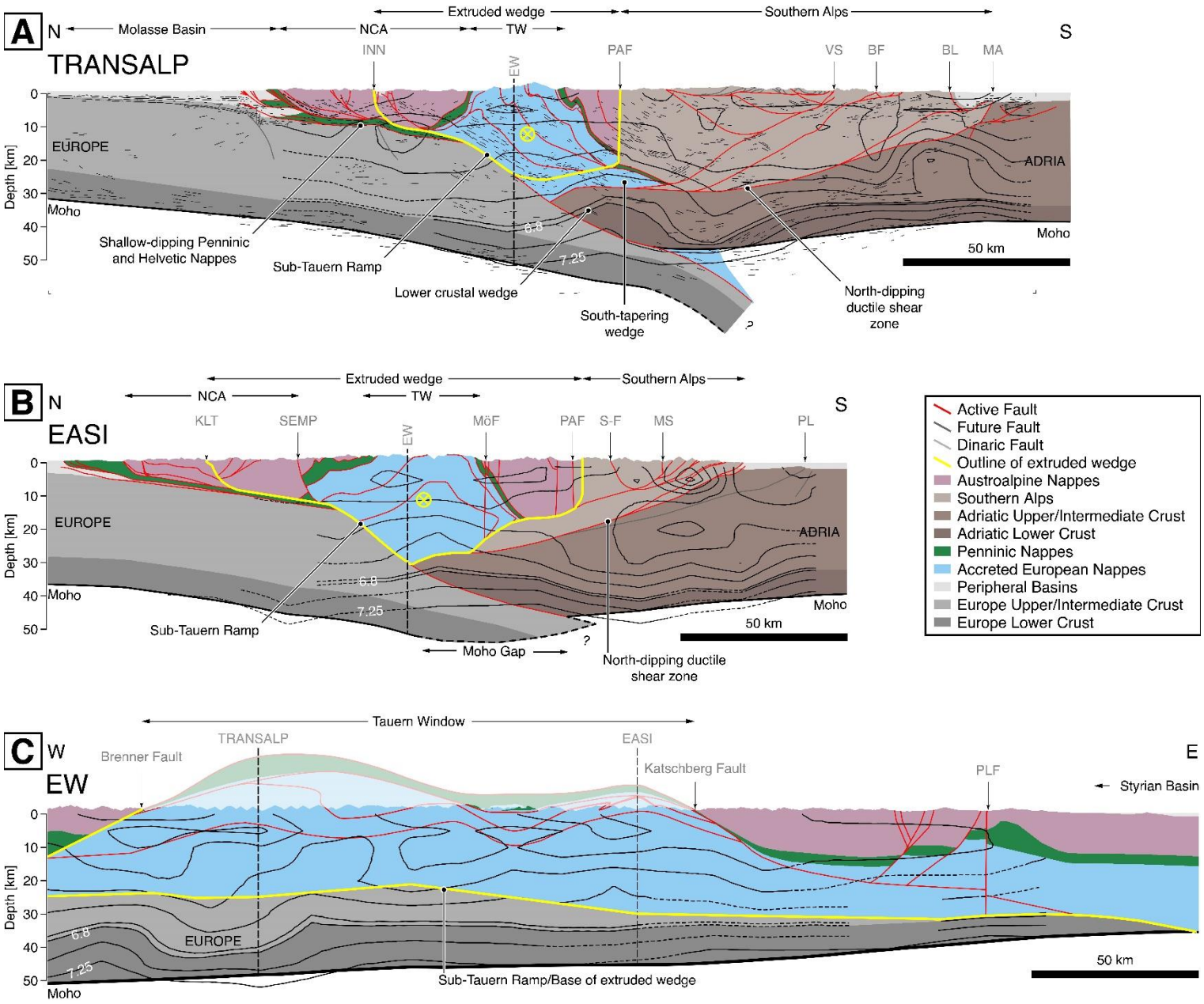

Figure 6: Present structure along the TRANSALP (A), EASI (B), and E-W (orogen-parallel) cross-sections (C), all shown at the same scale. Section traces in map-view are shown in Figure 2. LET contours at 0.25 km/s intervals on the sections are from Jozi Najafabadi et al. (2022). BL – Bassano Anticline; BF – Belluno Fault; IN – Inntal Fault; KLT – Königsee-Lammertal-Traunsee Fault; MA – Montello Anticline; MöF – Mölltal Fault; MS – Monte Simone Fault; NCA – North Calcareous Alps; PAF – Periadriatic Fault; SEMP – Salzach-Ennstal-Mariazell-Puchberg Fault; SF – Sava-Fella Fault; TW – Tauern Window; VS – Valsugana Fault.

Two features of the orogen-parallel section in Figure 6C stand out: 1) the eastward shallowing of the Moho from ~50 km below the Central Alps to ~35 km below the Styrian Basin, and even less to the east below the Pannonian Basin (Fig. 3B); and 2) the anomalous thickness of European-derived crust in the Tauern Window. This crust is thinned to the west and east in the footwalls of the Brenner and Katschberg normal faults, respectively. Comparing the orogen-parallel and orogen-normal sections, it is interesting to note that the anomalous thickness of intermediate European crust beneath the Tauern Window occurs immediately above and to the north of the lower crustal bulge overlying the gap between the Adriatic and European Mohos (Figs. 6A to C).

Present Mantle Structure

In Figure 7, we augment our model of the crustal structure with the P-wave teleseismic tomographic model of Paffrath et al. (2021) that images the upper mantle structure. A multitude of P-wave tomographic models are available for the Alpine and Carpathian domains (e.g., Bijwaard & Spakman, 2000; Karousova et al., 2013; Koulakov et al., 2009, 2009; Lippitsch, 2002; Serretti & Morelli, 2011; Zhu et al., 2015), but we chose Paffrath et al. (2021) because it uses three existing crustal velocity models (Diehl et al., 2009; Kennett et al., 1995; Tesauro et al., 2008) to arrive at an optimized crustal correction (see Paffrath et al. 2021 and their supplement for description). The high resolution afforded by this model is crucial for imaging structures in the depth interval of 60-150 km, which includes the transition from the orogenic crust to the lithospheric slabs beneath the Alps.

Positive velocity anomalies are generally interpreted as cooler and denser mantle lithosphere that either forms the base of the orogenic lithosphere and/or reaches further down as a slab into the asthenosphere. The asthenosphere is generally considered warmer and, therefore, marked by negative anomalies. However, we cannot rule out compositional heterogeneities as the cause of local variations in velocity (Fig. 7A).

In the TRANSALP section, the European lithosphere extends southwards beneath the orogenic lithosphere to at least 200 km (Fig.7A) depth. In contrast, no high-velocity slab anomaly is observed

beneath the EASI section (Fig. 7B). The latter section is marked by a discontinuity in the orogenic lithosphere between the European and Adriatic sides. This pronounced east-west change in the mantle structure in the TRANSALP and EASI sections is best seen in the orogen-parallel section (Fig. 7C), where the slab anomaly in the TRANSALP section gives way to the east to a low-velocity anomaly below the Tauern Window at a depth interval of approximately 70-150 km. This anomaly broadens from 12.5°E eastward towards the Pannonian Basin. The 1% velocity anomaly contour outlining the slab illustrates that the slab is largely disconnected from the overlying orogenic lithosphere.

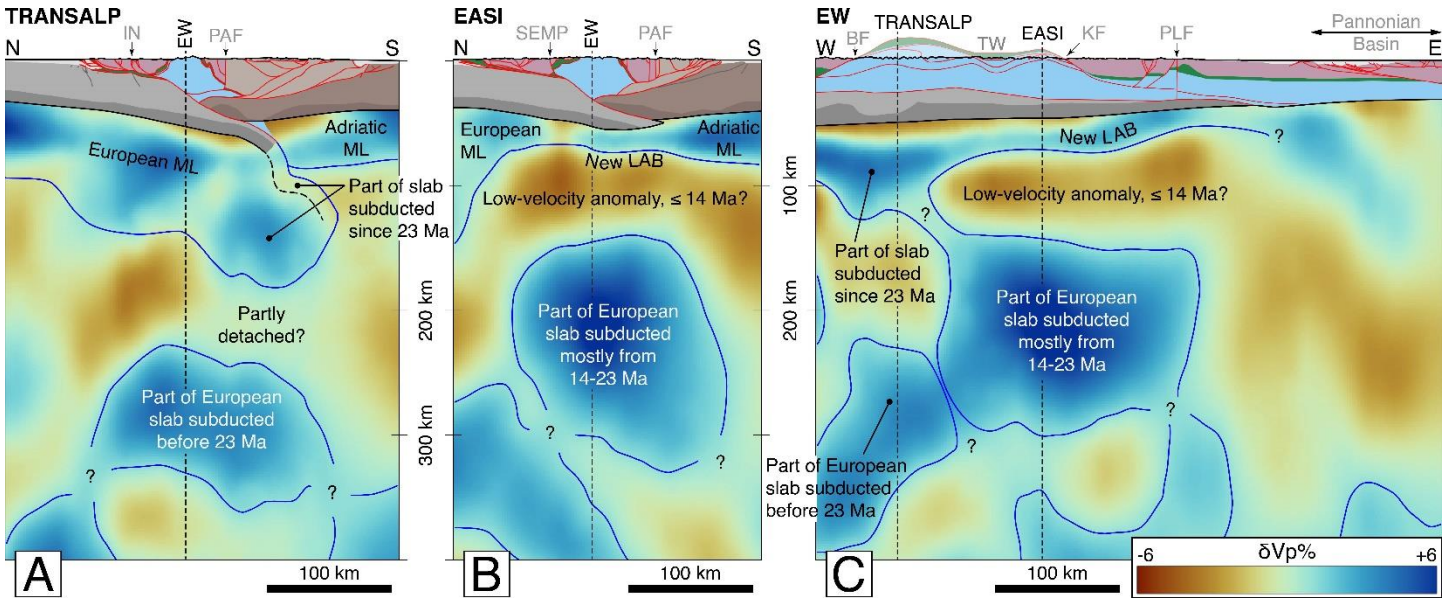

Figure 7: Structural model along the TRANSALP, EASI, and EW cross-sections, in relation to P-wave teleseismic tomography (Paffrath et al., 2021; we followed the common approach of smoothing model voxels using linear interpolation). The EW section reaches eastward to the Pannonian Basin, as defined by Miocene graben structures underlying the Plio-Pleostocene cover (see map trace in Fig. 2). Dashed dark grey lines mark intersections of the cross-sections. The blue lines closely follow the +1% anomaly contour line and outline the interpreted boundary between lithospheric and asthenospheric mantle. ML – Mantle lithosphere. The blue line subdividing the large positive anomaly in C is drawn according to geological criteria (see text in 7.3). Domains marked with "?" may be attributed to compositional variability and/or smearing of the image of the downgoing European lithospheric mantle. Labels indicating interpreted mantle structures are described in Chapter 7.3. See Figure 2 for cross-section traces in map view and Figure 6 for labelled structures in cross-sections. BF – Brenner Fault; IN – Inntal Fault; PAF – Periadriatic Fault; PLF – Pols-Lavanttal Fault.

6. Retrodeformation

TRANSALP

In the 14 Ma cross-section (Fig. 7B), we restore 46 km of N-S shortening in the Southern Alps fold-thrust belt above a north-dipping ductile shear zone. The shortened upper to middle crustal rocks are interpreted to have formed the cover of the Adriatic lower crustal wedge, which is imaged as a high-velocity anomaly in the LET data (Figs. 3 and 8). In the 0 Ma section (Fig. 7A), we interpret a south-tapering wedge of European crust (Figs. 8A and 8B, thrust slice labelled [2]) between the Adriatic lower crustal wedge and the Southern Alps (Fig. 8A, thrust slice labelled [1]). This out-of-sequence stacking of units is achieved by inferring that the Valsugana Fault cut down to the north and accreted this slice of European crust. Serravallian (~14-12 Ma) conglomerates preserved in its footwall (Castellarin et al. 1992) constrain thrusting to have occurred no earlier than 14 Ma.

We restore 17 km of N-S shortening accommodated by eastward orogen-parallel motion between the Periadriatic and Inntal faults (Fig. 4) from 14 – 0 Ma (Fig. 8B). North of the Inntal Fault, the Subalpine Molasse was shortened by 8 km from 23 – 9 Ma (Ortner et al., 2014). We assume that this was accommodated at a constant rate (0.6 km/Myr) and thus restore 3 km of shortening from 14 - 9 Ma. Together, these estimates add up to 66 km of shortening in the TRANSALP section since 14 Ma.

Going further back in time from 14 to 23 Ma, we restore 21 km of N-S shortening associated with orogen-parallel motion (Fig. 8C) including sinistral motion along the ZWD related to E-W stretching of the Austroalpine Nappes between the Tauern Window and Periadriatic Fault (Fig. 2; Scharf et al. 2013, Favaro et al., 2017). In the Tauern Window, the Venediger Nappes were affected by ductile folding and shearing under retrograde amphibolite-to-greenschist-facies conditions (Favaro et al., 2015). We restore 30 km of shortening by upright folding, treating the Venediger Nappes as a single unit with a fixed cross-sectional area. These nappes experienced E-W stretching, which in a N-S cross-section is represented by area loss. In the absence of constraints on the magnitude of this loss, we assume constant area, thereby slightly underestimating the actual area that the Venediger Nappes would have occupied in the TRANSALP section at 23 and 14 Ma.

In the Tauern Window, the Austroalpine Nappes that once formed the roof of the Venediger Nappes have been eroded (Favaro et al., 2017), so we calculate the vertical distance to the top of the Venediger Nappe stack at 23 Ma by using estimates of maximum burial (20 km) from geobarometry in post-nappe Barrovian metamorphism (0.7 GPa, Selverstone, 1993). Finally, we restore the European lower crust from the Sub-Tauern ramp, south of and below the unfolded Venediger Nappes (Figs. 8A and C). We restore 22 km of shortening north of the Inntal Fault, including 5 km in

the Subalpine Molasse. Taken together, the amount of N-S shortening between 23 and 14 Ma in the TRANSALP section amounts to 72 km. Thus, the total N-S shortening since 23 Ma is 138 km.

We note that the balancing of the TRANSALP section necessitates subducting a small piece of intermediate European crust (labelled [3] in Fig. 8A). In the absence of seismological evidence for this fragment, we arbitrarily placed it in the mantle wedge immediately south of the Moho gap between the European and Adriatic Plates. However, its precise location is unimportant for the purposes of this reconstruction.

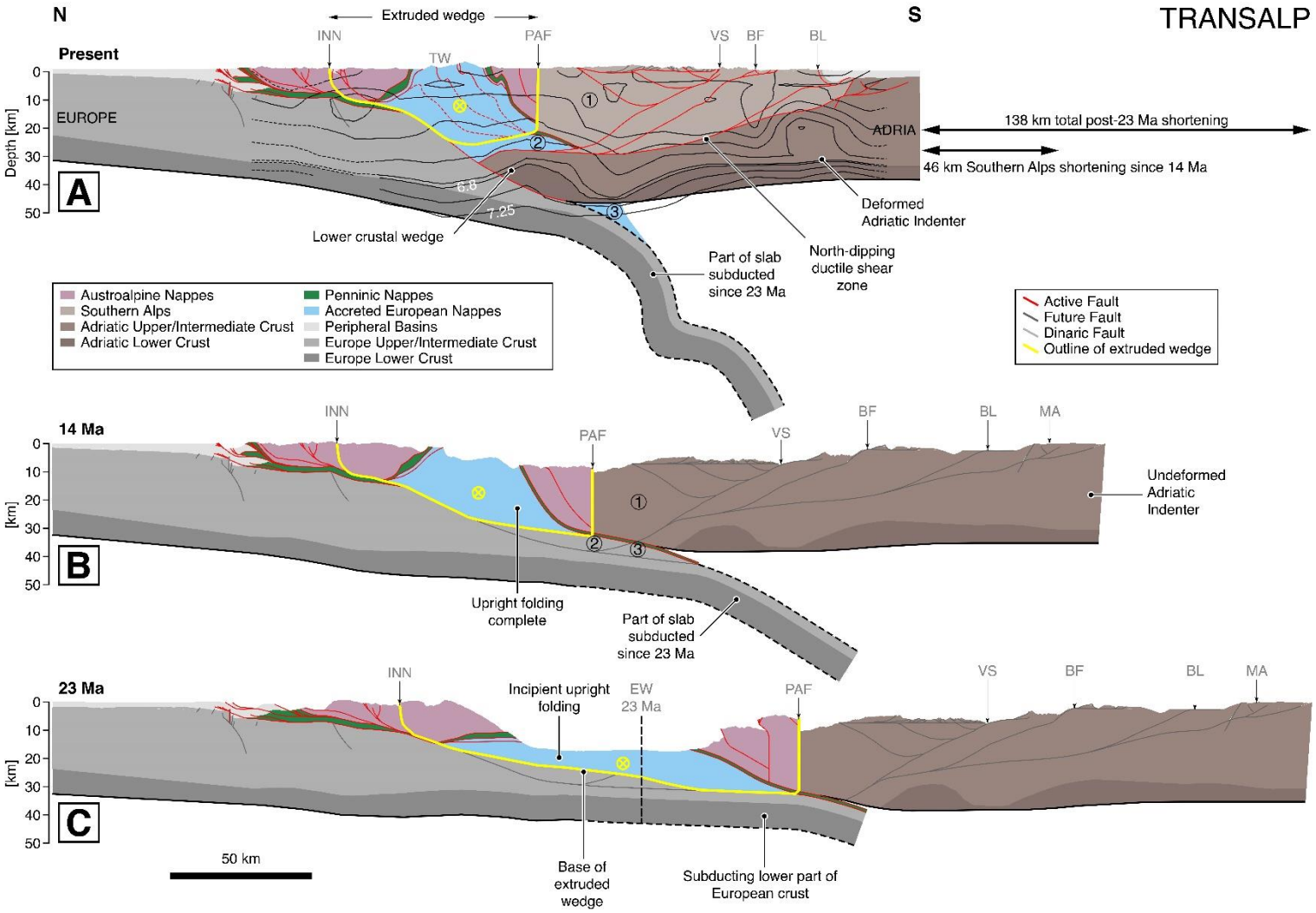

Figure 8: Restoration of the TRANSALP cross-section from the Present (A) back to 14 Ma (B) and 23 Ma (C). The slab geometry in A is based on P-wave teleseismic tomography (Fig. 7). The length of the restored part of the slab is that required to underpin the Venediger Nappes at 23 Ma, and is maintained from 23 Ma to present, illustrating the amount of European subduction since 23 Ma. LET velocity contours at intervals of 0.25 km/s are taken from Jozi-Najafabadi et al. (2021). Oblique-slip faults bounding the eastward extruding wedge are highlighted in yellow.

EASI

In the 14 Ma cross-section (Fig. 8B), we restore 49 km of shortening in the Southern Alps above a north-dipping ductile shear zone that forms the base of the deformed part of the Adriatic indenter. As in the TRANSALP cross-section, the shortened upper and middle crustal rocks of the Southern Alpine fold-and-thrust belt originally formed the hangingwall of the lower crustal wedge, which is imaged as a high-velocity anomaly in subsurface seismic images (Figs. 3C and 8A).

In both the 14 and 23 Ma sections (Figs. 8B, C), we account for orogen-parallel transport using laterally offset cross-sections (Fig. 4). Eastward orogen-parallel transport accommodated a total of 43 km of N-S shortening since 23 Ma, with 31 km of this N-S shortening accommodated from 23 to 14 Ma and an additional 12 km from 14 Ma to the present.

From the 14 Ma to the 23 Ma reconstruction in Figure 8C, we restore ~20 km shortening due to out-of-sequence thrusting below the North Calcareous Alps. This is required to accommodate shortening between 20 and 9 Ma associated with NE-translation of the North Calcareous Alps along the oblique-sinistral Inntal Fault once northward propagation of Subalpine Molasse thrusting had ceased (~20 Ma; Hinsch, 2013). Most of this out-of-sequence thrusting occurred within the Penninic and Helvetic nappes and by thrusting of the North Calcareous Alps over these nappes (Beidinger & Decker, 2014; Hinsch, 2013). Using the ~20 km estimate of out-of-sequence shortening, we restore the Penninic and Helvetic nappes as a single unit, preserving cross-sectional area. Poor surface exposure and a lack of internal reflectors in the seismic data presented in Hinsch (2013) make subsurface interpretation highly uncertain. As in the TRANSALP section, we extend the European lower crust below the unfolded Venediger Nappes.

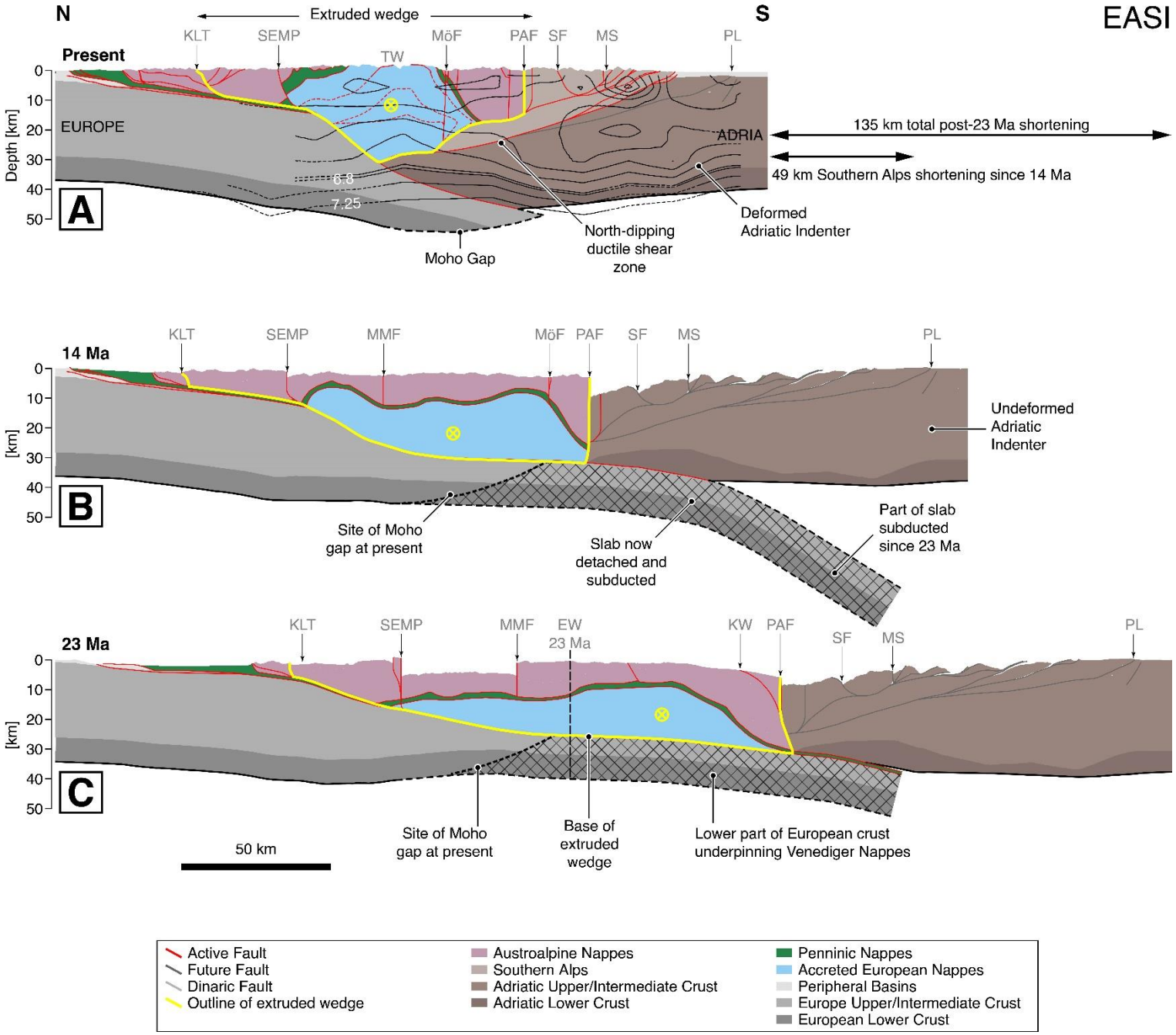

Figure 9: Restoration of the EASI cross-section from Present (A) back to 14 Ma (B) and 23 Ma (C). Faults bounding the eastwardly extruding wedge are highlighted in yellow. LET P-wave velocity contours at intervals of 0.25 km/s in (A) are taken from Jozi-Najafabadi et al. (2021). Tectonic units labelled 1-6 aid in the description of the retrodeformation in the text. The slab end in (A) is interpreted from P-wave teleseismic tomography, the location of the Moho gap, and LET P-wave velocity contours in Figure 7A. The cross-hatched grey area represents the European crust south of the present-day down-dip end of the positive velocity anomaly of the European slab. This end in (B) and (C) corresponds to the location of the Moho gap marked in (A), see text for discussion.

EW (orogen-parallel)

To restore the present EASI section in Figure 10A to 23 Ma (Fig. 10C), we first translate the section line (Fig. 2) southward to account for shortening by upright folding exposed in the Tauern Window (see Figs. 8C and 9C for intersection of the EW section with the TRANSALP and EASI cross-sections at 23 Ma). The thickness of the Venediger Nappes and subducting European crust is estimated by using the intersections with TRANSALP and EASI cross-sections (Figs. 8C and 9C). We then restore at total of 60 km of extension reported on the Brenner and Katschberg faults (Fügenschuh et al. 2012, Scharf et al., 2013; Wolff et al., 2021).

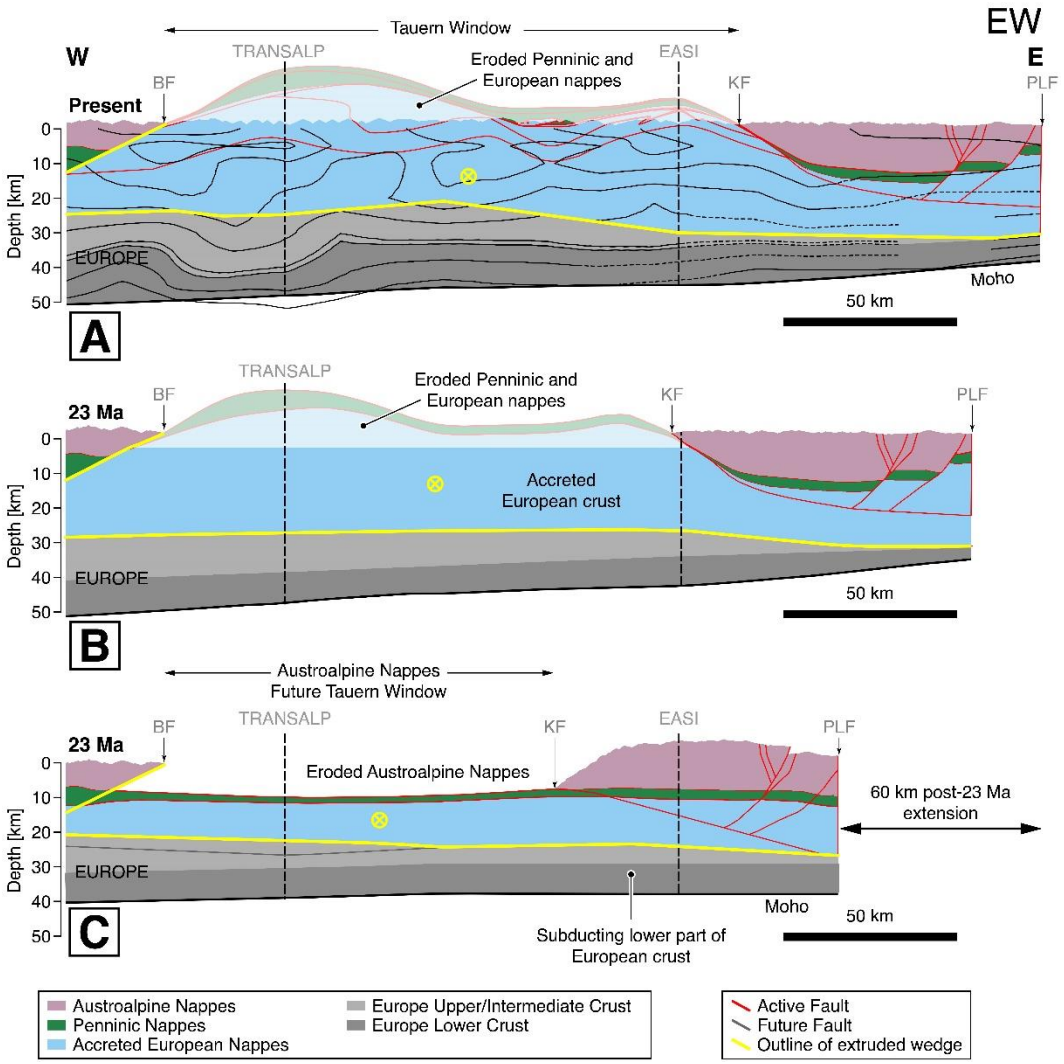

Figure 10: Restoration of the EW cross-section from Present (A) to 14 Ma (B), 23 Ma (B). Faults bounding the eastwardly extruding wedge are highlighted in yellow. LET contours at intervals of 0.25

km/s in (A) are taken from Jozi-Najafabadi et al. (2021). BF – Brenner Fault; KF – Katschberg Fault; PLF – Pols-Lavanttal Fault.

7. Behaviour of orogenic lithosphere during indentation

7.1 Timing of indentation and the mechanical response of the indented crust

Indentation of the Eastern Alps occurred in two phases, first involving the whole Adriatic crust during ~23-14 Ma, then followed by N-S shortening of the leading edge of the Adriatic Plate since 14 Ma. The first phase of indentation coincided with the cessation of the northward advance of the thrust front into the Molasse Basin, north of Salzburg (Fig. 2; Hinsch, 2013; Ortner et al., 2014). The Adriatic Indenter moved north along the northern segment of the Giudicarie Fault, displacing the Periadriatic Fault by some 70 km (e.g., Laubscher, 1990; Schönborn, 1992). This motion was largely accommodated by post-nappe, upright folding in the Tauern Window. The second phase entailed wedging of the Adriatic middle and lower crust into the base of the Eastern Alpine orogenic wedge.

Upright folding in the Tauern Window was broadly coeval with E-W extension on the Katschberg and Brenner faults, as argued on structural and thermochronological grounds by Fügenschuh et al. (1997), Scharf et al. (2013) and Rosenberg et al. (2018). This was linked to eastward extrusion of the high-grade metamorphic core of the Eastern Alpine orogen between conjugate, oblique strike-slip faults that transect the orogen (Fig. 2). In the TRANSALP and EASI sections for 23 Ma (Figs. 8C and 9C), we infer that these faults flatten into a common detachment surface (*sensu* Oldow et al., 1990) at the base of the Venediger Nappes at ~25 km depth as highlighted in yellow in Figures 8, 9, and 10. Above this basal detachment, we restore 67 km and 42 km of shortening in the TRANSALP and EASI cross-sections, respectively. Going from west to east along the Tauern Window, the proportion of N-S shortening accommodated by upright folding decreases and the proportion of shortening by orogen-parallel transport increases. Rosenberg et al. (2018, their Fig. 23) schematically illustrated how a series of easterly diverging conjugate strike-slip faults account for these trends. In the western Tauern Window, orogen-parallel transport was accommodated primarily the Inntal and Periadriatic faults only. In the eastern Tauern Window, the SEMP, ZWD, and Mölltal Faults accommodated additional orogen-parallel transport (Fig. 4), leading to an eastward increase in orogen-parallel displacement relative to the European foreland and thus an eastward increase in shortening taken up by orogen parallel motion. A consequence of placing the basal detachment at the base of the Venediger Nappes (Figs. 8, 9, and 10) is that shortening in the east was accommodated without

significant crustal thickening, whereas in the west, south-directed subduction of the European lithosphere accommodated N-S convergence of the underlying lower crust and mantle lithosphere.

The Venediger Nappes were affected by Barrow-type metamorphism between 32-25 Ma, resulting in temperatures of 500-600°C (e.g., Favaro et al., 2017; Schuster et al., 2004). Given the strong temperature sensitivity of crustal viscosity (e.g., Carter et al., 1987; Handy, 1989; Kohlstedt et al., 1995), high temperatures are expected to have reduced the viscous strength of the nappe pile in the Tauern Window during burial in Paleogene time. During subsequent indentation, upright isoclinal folding rotated the main foliation into increasingly high angles with the direction of indentation, thus increasing the bulk viscous strength of the Venediger Nappes in the N-S direction of indentation, an effect known in rock mechanics as geometric- or foliation-hardening. The nappes are expected to have strengthened even more as they exhumed and cooled below 300°C, i.e., through the viscous-to-frictional transition in granitoid rocks (e.g., Handy et al., 1999). Strengthening rendered the nappe stack a strong body that resisted further indentation, such that N-S convergence was increasingly accommodated by south-directed folding and thrusting in the Dolomites Indenter, forming the eastern Southern Alps.

7.2 Crustal wedging

During the second phase of indentation, a ductile shear zone in the Southern Alpine basement accommodated northward wedging of the Adriatic middle-to-lower crust above subducted European lithosphere in the TRANSALP and EASI sections (Figs 8, 9). This wedging is kinematically like the wedging proposed for the NFP-20E section west of the Giudicarie Fault (e.g., Schmid et al., 1996, and references therein, see also Rosenberg & Kissling, 2013). In contrast to the NFP-20E section, however, the indented orogenic wedge east of the Giudicarie Fault comprises both accreted European and Adriatic units. The latter were emplaced as nappes during late Cretaceous and Paleogene accretion and subduction (Schmid et al., 2004; Schuster et al., 2004), i.e., prior to Neogene indentation.

The model of crustal indentation and European subduction in Figures 6A and 6B differs markedly from past interpretations in which the middle to lower crust of the eastern Southern Alps was subducted on a north-dipping slab of Adriatic lithosphere (e.g., Handy et al., 2015; Lippitsch, 2002; Schmid et al., 2004). Here, we follow Mitterbauer et al. (2011) in interpreting the positive P-wave velocity anomaly beneath the Eastern Alps as a remnant of the subducted European Plate. Handy et al. (2021) argued against an Adriatic origin for this slab because its 100-200 km down-dip length far exceeds shortening in the Southern Alps (Figs. 8 and 9; Castellarin et al., 1998).

North of the Periadriatic Fault, we find around 90 km total shortening (92 km in TRANSALP, Fig. 8; 86 km in EASI, Fig. 9). This shortening, involving European-accreted nappes, occurred above the European lithosphere (Figs. 6A, 6B, 8 and 9), requiring subduction equivalent to the shortening we reconstruct. Along the TRANSALP cross-section, the slab corresponding to this shortening is imaged as a south-dipping positive velocity anomaly in teleseismic P-wave tomography (Fig. 7A). European subduction must have been continuous but slow throughout the Neogene to accommodate Adriatic indentation that involved upright folding, orogen-parallel extrusion, and orogen-normal thrusting.

7.3 Constraints on subduction and possible slab detachment events

The approximate age of the positive velocity anomalies that are interpreted as subducted slabs can be constrained by comparing the current slab lengths in Figure 7 with the amount of N-S shortening estimated from the three-dimensionally balanced cross sections in Figures 8 and 9. In so doing, we assume that lithospheric volume is conserved during subduction. Crustal shortening estimates obtained by retrodeforming nappe systems must always be regarded as minima in the absence of both adequate cutoff markers and evidence precluding subduction erosion. Also, slab lengths are difficult to measure and compare in teleseismic tomographic images, not only due to poor resolution and smearing of the images (e.g., Foulger 2013), but also because slabs themselves may be deformed (Lister et al. 2008). In the model used here (Paffrath et al. 2021), the reported vertical resolution is about 20 km down to c. 150 km depth and decreases to 50 km at greater depth, with considerable smearing at depths down to c. 350 km, the maximum depth considered here. Despite these limitations, the combined geological-geophysical approach below yields general insight into the possible volumes and ages of subducted lithosphere beneath the Eastern Alps.

The south-dipping slab anomaly in the TRANSALP section (Fig. 7A) is at least 200 km long, exceeding the 138 km of post-23 Ma N-S shortening estimated above along this section (Fig. 8). Some of this difference may be attributed to stretching of the down-going slab under its own weight (e.g., Lister et al. 2008), but the estimates are similar enough to indicate that the slab still attached to the orogenic lithosphere represents lithosphere mostly subducted since 23 Ma. The down-dip end of this anomaly may therefore represent a detachment surface at about 23 Ma. Extensive analysis of tomographic slices in this area indicates that this high-velocity anomaly actually connects out-of-section with the vertically underlying positive anomaly at 220-350 km depth. This is inferred to comprise lithosphere that subducted mostly before 23 Ma, i.e., in Paleogene time (Fig. 7A).

In contrast, the EASI section lacks a slab anomaly and instead features only a thin high velocity layer beneath the Moho (Fig. 7B). Thus, there is no slab still attached to the orogenic lithosphere to

accommodate the total of 135 km of N-S shortening in this section since 23 Ma (Figs. 9B and 9C). The only plausible candidate for this slab is the positive anomaly in Figures 7B and 7C entrained between 150 and 300 km depth. In the EASI section, the ~150 km down-dip length of this anomaly exceeds the aforementioned amount of post-23 Ma shortening by only 15 km. Taken at face value, the excess length of the anomaly indicates either that the slab underwent down-dip stretching and/or that it includes some 15 km of European lithosphere that was subducted before 23 Ma. Thus, like the TRANSALP section, the bottom of the anomaly in the EASI section may lie at or near a slab detachment surface at 23 Ma.

The western part of this large anomaly, which is the same positive anomaly imaged between 220-350 km depth in the TRANSALP section (Fig. 7a), is inferred to comprise older lithosphere subducted prior to 23 Ma based on the arguments above. Thus, by applying areal balancing of crustal shortening, we surmise that what appears as a single large positive anomaly in Figure 7C is actually a segmented slab. Lines delineating older and younger segments are drawn accordingly in Figure 7C. Lines delineating older and younger segments are drawn accordingly in Figure 7C. The resolution of the P-wave tomographic model used here (Paffrath et al. 2021) is insufficient to distinguish closely spaced slab segments at this depth.

Shallow removal of the slab in EASI section must have occurred after 23 Ma, possibly even after 14 Ma to account for the lack of slab to accommodate the 68 km of post-14 Ma N-S shortening estimated above (Fig. 9A, 9B). Shallow slab removal earlier than 14 Ma can be ruled out because asthenosphere would have been emplaced in direct contact with the base of the Venediger Nappes (cross-hatched area in Figs. 9B and 9C). This is implausible in the absence of mid-Miocene metamorphism and volcanism in the Eastern Alps (e.g., Göğüş & Pysklywec, 2008; Reid et al., 2017). Therefore, we ascertain that European lithosphere in the upper part of the detached slab in the EASI section formed the substratum of the Venediger Nappes beneath the Sub-Tauern Ramp until sometime after 14 Ma when it was removed.

In keeping with this scenario, we interpret the thin high-velocity anomaly beneath the EASI section to be newly formed mantle lithosphere (marked new LAB in Figs. 7B, 7C) that has grown since the last slab removal event at ≤ 14 Ma. The negative velocity anomaly in P-wave tomography in the depth interval of 70-150 km of the EASI section (Figs. 7B, 7C) is thought to represent asthenosphere filling the subhorizontal gap left by this slab removal. Notably, this negative velocity anomaly does not extend as far west as the TRANSALP section. It neither coincides with the northern projection of the Giudicarie Fault (Figs. 2 and 7C), nor does it line up with the eastern and western ends of the

Tauern Window. This discrepancy in the location of crustal and mantle structures suggests that the major faults exposed at the surface formed before slab removal at ≤ 14 Ma as argued below.

To conclude this section, there was one, possibly two slab removal events in the Eastern Alps, the first at 23 Ma marked in both the TRANSALP and EASI sections by the down-dip ends of high-velocity anomalies, and the second only in the EASI section marked by the accretion of a new thin lithospheric mantle above upwelling of asthenosphere corresponding to a shallow negative velocity anomaly (Fig. 7C).

7.4 Geological expression of slab removal events

What is the geological expression of the slab removal events inferred above from tectonic balancing and P-wave seismic tomography? Partial detachment of subducting European lithosphere in early Miocene time would fit well with previous proposals of slab detachment (Handy et al., 2015, 2021; Schlunegger & Kissling, 2022) to explain sudden tectonic uplift and infilling of the marine eastern Molasse Basin in Burdigalian time e.g., Hülscher et al., 2019; Kuhlemann & Kempf, 2002; Le Breton et al., 2023). This uplift may represent the terminal stages of slab detachment that began at ~23 Ma, facilitating the indentation and orogen-parallel extension of the Eastern Alps, as well as triggering extension in the Pannonian Basin in the upper plate of the retreating Carpathian subduction orogen. It may also have initiated the mid-Miocene change in orogenic polarity from N-directed thrusting along the northern front of the eastern Alps to S-directed folding and thrusting in the Southern Alps. These events immediately predated and were continuous with the ~20 Ma onset of major east-west extension in the Pannonian Basin that accompanied roll-back subduction in the Carpathians (~200-300 km; e.g., Royden & Burchfiel, 1989; Horváth et al., 2006, 2015; Ustaszewski et al., 2008). Thus, Adriatic indentation rather than Carpathian roll-back subduction was the probably trigger of orogen-parallel extension in the Eastern Alps (Scharf et al. 2013, Schmid et al. 2013).

Evidence for removal of part of the European slab beneath the Eastern Alps after 14 Ma is more difficult to find in the geologic record. The eastern Molasse Basin underwent 500-900 m of post-Late Miocene erosion (Gusterhuber et al., 2012) that has been tied to 200-600 m of Late Mio-Pliocene tectonic uplift (Genser et al., 2007, Le Breton et al. 2023). However, this erosion and uplift also affected the western and central Molasse Basin (e.g., Baran et al., 2014; Cederbom et al., 2011), and thus cannot be unequivocally linked to slab detachment beneath the Eastern Alps. Higher exhumation rates (~700 m/Myr) in the Eastern Alps are restricted to the western Tauern Window (e.g., Bertrand et al., 2017; Fox et al., 2015; Heberer et al., 2017), just west of the proposed locus of

slab removal. Some authors argue that post-glacial isostatic rebound explains current surface uplift rates of ~1 mm/yr in the Eastern Alps (Mey et al., 2016; Sternai et al., 2019).

Another explanation is that low subduction rates (3-4 mm/yr average based on our shortening estimates) may have allowed the slab to heat up as Adria-Europe convergence ground to a halt. This may have promoted thermal erosion, and would have decreased the viscosity of the slab, rendering it more deformable while gradually increasing its buoyancy and decreasing slab-pull. Taken together, these factors would be expected to reduce the rates and amounts of response to slab removal, making it difficult if not impossible to distinguish at the surface.

Finally, we note that Neogene slab detachment(s) does not preclude an older slab detachment event in Eo-Oligocene time, which has long been proposed to explain calc-alkaline magmatism along the Periadriatic Fault (Von Blanckenburg & Davies, 1995) and rapid uplift and erosion of the retro-wedge of the Central Alps e.g., Schlunegger & Castelltort, 2016; Sinclair, 1997). Thus, the Eastern Alps may well have witnessed up to three late- to post-collisional slab detachment events, resulting in the complex three-dimensional slab geometries imaged today by P-wave tomography in the AlpArray experiment.

8. Conclusions

We have reconstructed the Neogene to Present structural evolution of the Eastern Alps in N-S (TRANSALP, EASI) and E-W (orogen-parallel) cross-sections of the orogenic wedge that are corrected for out-of-section orogen-parallel transport. Correlating these three-dimensionally balanced sections with the geological record reveals two phases of Adriatic indentation of the Eastern Alpine orogenic wedge. During these phases, the total N-S shortening of ~135 km north of the Periadriatic Fault in both the TRANSALP and EASI transects was accommodated by a roughly equivalent amount of subduction of European lithosphere.

The first phase of indentation (~23-14 Ma), concurrent with the termination of northward thrust advancement into the Molasse Basin, involved the northward movement of the Dolomites sub-indenter of the Adriatic Plate along the Giudicarie Fault. This movement displaced the Periadriatic Fault by some 70 km and was accompanied by post-nappe upright folding, and E-W extension in the Tauern Window. The latter was broadly coeval with eastward orogen-parallel transport (Scharf et al. 2013, Rosenberg et al. 2018) at an average rate of ≥ 4 mm/yr. We propose that this first phase of

indentation as having been triggered by detachment of the European slab beneath large parts of the Eastern Alps beginning at 23 Ma.

The second phase of indentation (~14-0 Ma) involved deformation of the leading edge of the Adriatic indenter, forming the Southern Alps fold-thrust belt as the Adriatic middle-to-lower crust wedged into the base of the Eastern Alpine orogenic wedge. We tentatively relate this second phase of indentation to gradual removal of the part of the European slab remaining after the earlier detachment event. There is no unequivocal surface expression of this late slab removal event, possibly indicating that the slab load was modest released by earlier detachment.

In parting, we note that our exploration of the consequences of slab removal on the orogenic crust involved using only the P-wave tomographic model (Paffrath et al. 2021), Yet, differences remain among seismological models, both between models based on different methods and among models using the same method in the Alps (Kästle et al., 2020). These differences are most pronounced in the crucial depth interval between 70 and 150 km (Paffrath et al. 2021). This underscores the need for rigorous benchmarking of seismological models (e.g., Kästle & Paffrath, 2023), which may help us to ascertain whether tomographic images portray a physical reality or merely reflect the myriad assumptions made in collecting, processing, and inverting seismic waveforms. Using geological data on the age and kinematics of crustal motion provides an independent means of testing the viability of seismological models.

Acknowledgements

We acknowledge the generous support of the German Science Foundation (DFG) in the form of research grant Ha 2403/23-2 to the second author. This grant supported the first author and all coordination activities of the research priority program SPP-2017 entitled “Mountain Building in 4-Dimensions (4D-MB)”. Our sincere thanks also go to many colleagues in 4D-MB, amongst them those who took the time to discuss, but do not necessarily agree with, the conclusions reached here: Eline Le Breton, Marcel Paffrath, Stefan Schmid, Emanuel Kästle, Christian Haberland, Azam Jozi Najafabadi, Klaus Bauer. We thank PE Ltd for donating academic licences for *Move*™ structural modelling and analysis software.

Data availability statement

Local earthquake tomography data are available through Jozi Najafabadi et al. (2022). P-wave teleseismic tomography data are available through Paffrath et al. (2021). Reflection seismic data are

available through Lüschen et al. (2006). Geological map data used in cross-section construction are listed in supporting information S1-3.

References

AlpArray Seismic Network Team, AlpArray OBS Cruise Crew, AlpArray Working Group, Hetényi, G., Molinari, I., Clinton, J., Bokelmann, G., Bondár, I., Crawford, W. C., Dessa, J.-X., Doubre, C., Friederich, W., Fuchs, F., Giardini, D., Gráczer, Z., Handy, M. R., Herak, M., Jia, Y., Kissling, E., … Živčić, M. (2018). The AlpArray Seismic Network: A Large-Scale European Experiment to Image the Alpine Orogen. *Surveys in Geophysics*, *39*(5), 1009–1033. https://doi.org/10.1007/s10712-018-9472-4

Anderlini, L., Serpelloni, E., Tolomei, C., De Martini, P. M., Pezzo, G., Gualandi, A., & Spada, G. (2020). New insights into active tectonics and seismogenic potential of the Italian Southern Alps from vertical geodetic velocities. *Solid Earth*, *11*(5), 1681–1698. https://doi.org/10.5194/se-11-1681-2020

Auer, M., & Eisbacher, G. H. (2003). Deep structure and kinematics of the Northern Calcareous Alps (TRANSALP Profile). *International Journal of Earth Sciences*, *92*(2), 210–227. https://doi.org/10.1007/s00531-003-0316-0

Bachmann, G. H., & Müller, M. (1981). Geologie der Tiefbohrung Vorderriß I (Kalkalpen, Bayern). *Geologica Bavarica*, *81*(Die Tiefbohrung Vorderriß I (Kalkalpen, Bayern)), 17–53.

Baran, R., Friedrich, A. M., & Schlunegger, F. (2014). The late Miocene to Holocene erosion pattern of the Alpine foreland basin reflects Eurasian slab unloading beneath the western Alps rather than global climate change. *Lithosphere*, *6*(2), 124–131. https://doi.org/10.1130/L307.1

Battista Carulli, G., Della Vedova, B., Podda, F., Slejko, D., & Zanolla, C. (2006). *Carta Geologica del Friuli Venezia Giulia* [Map]. Servizio Geologico Regione Autonoma Friuli Venezia Giulia.

Bauer, K., Schwarz, B., Trichandi, R., Wawerzinek, B., McPhee, P., & Handy, M. R. (2024, March 8). *New insights into seismic structures around the Tauern Window and the Periadriatic Fault System from reprocessing of TRANSALP seismic reflection data*. https://doi.org/10.5194/egusphere-egu24-11066

Beidinger, A., & Decker, K. (2014). Quantifying Early Miocene in-sequence and out-of-sequence thrusting at the Alpine-Carpathian junction: Reconstruction of thrusting Eastern Alps. *Tectonics*, *33*(3), 222–252. https://doi.org/10.1002/2012TC003250

Bertotti, G., Siletto, G. B., & Spalla, M. I. (1993). Deformation and metamorphism associated with crustal rifting: The Permian to Liassic evolution of the Lake Lugano-Lake Como area (Southern Alps). *Tectonophysics*, *226*(1), 271–284. https://doi.org/10.1016/0040-1951(93)90122-Z

Bertrand, A., Rosenberg, C., Rabaute, A., Herman, F., & Fügenschuh, B. (2017). Exhumation mechanisms of the Tauern Window (Eastern Alps) inferred from apatite and zircon fission track thermochronology: EXHUMATION OF THE TAUERN WINDOW. *Tectonics*, *36*(2), 207–228. https://doi.org/10.1002/2016TC004133

Bianchi, I., Ruigrok, E., Obermann, A., & Kissling, E. (2021). Moho topography beneath the European Eastern Alps by global-phase seismic interferometry. *Solid Earth*, *12*(5), 1185–1196. https://doi.org/10.5194/se-12-1185-2021

Bijwaard, H., & Spakman, W. (2000). Non-linear global *P* -wave tomography by iterated linearized inversion. *Geophysical Journal International*, *141*(1), 71–82. https://doi.org/10.1046/j.1365-246X.2000.00053.x

Bleibinhaus, F., & Groschup, R. (2008). *Structure of the Periadriatic Fault in the Eastern Alps from reflection seismic imaging*. American Geophysical Union, Fall Meeting 2008, San Francisco.

Brack, P. (1981). Structures in the southwestern border of the Adamello intrusion (Alpi Bresciane, Italy). *Schweizerische Mineralogische Und Petrographische Mitteilungen*, *61*(1), 37–49. https://doi.org/10.5169/seals-47129

Bressan, G., Ponton, M., Rossi, G., & Urban, S. (2016). Spatial organization of seismicity and fracture pattern in NE Italy and W Slovenia. *Journal of Seismology*, *20*(2), 511–534. https://doi.org/10.1007/s10950-015-9541-9

Buiter, S. J. H., Govers, R., & Wortel, M. J. R. (2002). Two-dimensional simulations of surface deformation caused by slab detachment. *Tectonophysics*, *354*(3–4), 195–210. https://doi.org/10.1016/S0040-1951(02)00336-0

Burke, M. M., & Fountain, D. M. (1990). Seismic properties of rocks from an exposure of extended continental crust—New laboratory measurements from the Ivrea Zone. *The Nature of the Lower Continental Crust*, *182*(1), 119–146. https://doi.org/10.1016/0040-1951(90)90346-A

Castellarin, A., & Cantelli, L. (2000). Neo-Alpine evolution of the Southern Eastern Alps. *Journal of Geodynamics*, *30*(1–2), 251–274. https://doi.org/10.1016/S0264-3707(99)00036-8

Castellarin, A., Luigi, S., Picotti, V., & Cantelli, L. (1998). La tettonica delle Dolomiti nel quadro delle Alpi Meridionali Orientali. *Mem. Soc. Geol. Ital.*, *53*, 133–143.

Cederbom, C. E., Van Der Beek, P., Schlunegger, F., Sinclair, H. D., & Oncken, O. (2011). Rapid extensive erosion of the North Alpine foreland basin at 5-4 Ma: Rapid extensive erosion of the North Alpine foreland basin. *Basin Research*, *23*(5), 528–550. https://doi.org/10.1111/j.1365-2117.2011.00501.x

Diehl, T., Husen, S., Kissling, E., & Deichmann, N. (2009). High-resolution 3-D *P* -wave model of the Alpine crust. *Geophysical Journal International*, *179*(2), 1133–1147. https://doi.org/10.1111/j.1365-246X.2009.04331.x

Doglioni, C., & Bosellini, A. (1987). Eoalpine and mesoalpine tectonics in the Southern Alps. *Geologische Rundschau*, *76*(3), 735–754. https://doi.org/10.1007/BF01821061

Duretz, T., Gerya, T. V., & May, D. A. (2011). Numerical modelling of spontaneous slab breakoff and subsequent topographic response. *Tectonophysics*, *502*(1–2), 244–256. https://doi.org/10.1016/j.tecto.2010.05.024

Eizenhöfer, P. R., Glotzbach, C., Kley, J., & Ehlers, T. A. (2023). Thermo-Kinematic Evolution of the Eastern European Alps Along the TRANSALP Transect. *Tectonics*, *42*(4), e2022TC007380. https://doi.org/10.1029/2022TC007380

Elias, J. (1998). *The thermal history of the Ötztal Stubai complex (Tyrol, Austria, Italy) in the light of the lateral extrusion model*. Inst. und Museum für Geologie und Paläontologie Tübingen; WorldCat.

Favaro, S., Handy, M. R., Scharf, A., & Schuster, R. (2017). Changing patterns of exhumation and denudation in front of an advancing crustal indenter, Tauern Window (Eastern Alps): Indentation, Exhumation and Denudation. *Tectonics*, *36*(6), 1053–1071. https://doi.org/10.1002/2016TC004448

Favaro, S., Schuster, R., Handy, M. R., Scharf, A., & Pestal, G. (2015). Transition from orogen-perpendicular to orogen-parallel exhumation and cooling during crustal indentation—Key constraints from 147Sm/144Nd and 87Rb/87Sr geochronology (Tauern Window, Alps). *Tectonophysics*, *665*, 1–16. https://doi.org/10.1016/j.tecto.2015.08.037

Fodor, L., Jelen, B., Márton, E., Skaberne, D., Čar, J., & Vrabec, M. (1998). Miocene-Pliocene tectonic evolution of the Slovenian Periadriatic fault: Implications for Alpine-Carpathian extrusion models. *Tectonics*, *17*(5), 690–709. https://doi.org/10.1029/98TC01605

Fox, M., Herman, F., Kissling, E., & Willett, S. D. (2015). Rapid exhumation in the Western Alps driven by slab detachment and glacial erosion. *Geology*, *43*(5), 379–382. https://doi.org/10.1130/G36411.1

Frisch, W., Dunkl, I., & Kuhlemann, J. (2000). Post-collisional orogen-parallel large-scale extension in the Eastern Alps. *Tectonophysics*, *327*(3–4), 239–265. https://doi.org/10.1016/S0040-1951(00)00204-3

Frisch, W., & Gawlick, H.-J. (2003). The nappe structure of the central Northern Calcareous Alps and its disintegration during Miocene tectonic extrusion—A contribution to understanding the orogenic evolution of the Eastern Alps. *International Journal of Earth Sciences*, *1*(1), 1–1. https://doi.org/10.1007/s00531-003-0357-4

Fügenschuh, B. (1995). *Thermal and kinematic history of the Brenner area (Eastern Alps, Tyrol)*. ETH Zurich.

Fügenschuh, B., Seward, D., & Mancktelow, N. (1997). Exhumation in a convergent orogen: The western Tauern window. *Terra Nova*, *9*(5–6), 213–217. https://doi.org/10.1111/j.1365-3121.1997.tb00015.x

Garzanti, E., Radeff, G., & Malusà, M. G. (2018). Slab breakoff: A critical appraisal of a geological theory as applied in space and time. *Earth-Science Reviews*, *177*, 303–319. https://doi.org/10.1016/j.earscirev.2017.11.012

Genser, J., Cloetingh, S. A. P. L., & Neubauer, F. (2007). Late orogenic rebound and oblique Alpine convergence: New constraints from subsidence analysis of the Austrian Molasse basin. *Global and Planetary Change*, *58*(1–4), 214–223. https://doi.org/10.1016/j.gloplacha.2007.03.010

Göğüş, O. H., & Pysklywec, R. N. (2008). Mantle lithosphere delamination driving plateau uplift and synconvergent extension in eastern Anatolia. *Geology*, *36*(9), 723. https://doi.org/10.1130/G24982A.1

Groß, P., Handy, M. R., John, T., Pestal, G., & Pleuger, J. (2020). Crustal-Scale Sheath Folding at HP Conditions in an Exhumed Alpine Subduction Zone (Tauern Window, Eastern Alps). *Tectonics*, *39*(2), e2019TC005942. https://doi.org/10.1029/2019TC005942

Groß, P., Pleuger, J., & Handy, M. R. (2022). Rift-related paleogeography of the European margin in the Eastern Alps (Central Tauern Window). *Swiss Journal of Geosciences*, *115*(1), 27. https://doi.org/10.1186/s00015-022-00426-9

Gusterhuber, J., Dunkl, I., Hinsch, R., Linzer, H.-G., & Sachsenhofer, R. (2012). Neogene uplift and erosion in the Alpine Foreland Basin (Upper Austria and Salzburg). *Geologica Carpathica*, *63*(4), 295–305. https://doi.org/10.2478/v10096-012-0023-5

Handy, M. R., Franz, L., Heller, F., Janott, B., & Zurbriggen, R. (1999). Multistage accretion and exhumation of the continental crust (Ivrea crustal section, Italy and Switzerland). *Tectonics*, *18*(6), 1154–1177. https://doi.org/10.1029/1999TC900034

Handy, M. R., Giese, J., Schmid, S. M., Pleuger, J., Spakman, W., Onuzi, K., & Ustaszewski, K. (2019). Coupled Crust-Mantle Response to Slab Tearing, Bending, and Rollback Along the Dinaride-Hellenide Orogen. *Tectonics*, *38*(8), 2803–2828. https://doi.org/10.1029/2019TC005524

Handy, M. R., M. Schmid, S., Bousquet, R., Kissling, E., & Bernoulli, D. (2010). Reconciling plate-tectonic reconstructions of Alpine Tethys with the geological–geophysical record of spreading and subduction in the Alps. *Earth-Science Reviews*, *102*(3–4), 121–158. https://doi.org/10.1016/j.earscirev.2010.06.002

Handy, M. R., & Oberhänsli, R. (2004). Explanatory Notes to the Map: Metamorphic Structure of the Alps Age Map of the Metamorphic Structure of the Alps – Tectonic Interpretation and Outstanding Problems. *Mitteilungen Der Österreichischen Mineralogischen Gesellschaft*, *149*, 201–225.

Handy, M. R., Schmid, S. M., Paffrath, M., Friederich, W., & the AlpArray Working Group. (2021). Orogenic lithosphere and slabs in the greater Alpine area – interpretations based on teleseismic P-wave tomography. *Solid Earth*, *12*(11), 2633–2669. https://doi.org/10.5194/se-12-2633-2021

Handy, M. R., Ustaszewski, K., & Kissling, E. (2015). Reconstructing the Alps–Carpathians–Dinarides as a key to understanding switches in subduction polarity, slab gaps and surface motion. *International Journal of Earth Sciences*, *104*(1), 1–26. https://doi.org/10.1007/s00531-014-1060-3

Heberer, B., Reverman, R. L., Fellin, M. G., Neubauer, F., Dunkl, I., Zattin, M., Seward, D., Genser, J., & Brack, P. (2017). Postcollisional cooling history of the Eastern and Southern Alps and its linkage to Adria indentation. *International Journal of Earth Sciences*, *106*(5), 1557–1580. https://doi.org/10.1007/s00531-016-1367-3

Heit, B., Cristiano, L., Haberland, C., Tilmann, F., Pesaresi, D., Jia, Y., Hemmleb, S., Haxter, M., Zieke, T., Jaeckl, K.-H., Schloemer, A., & Weber, M. (2023). *The SWATH-D seismological network in the Eastern Alps*. 1 S. https://doi.org/10.17169/REFUBIUM-41105

Hetényi, G., Plomerová, J., Bianchi, I., Kampfová Exnerová, H., Bokelmann, G., Handy, M. R., & Babuška, V. (2018). From mountain summits to roots: Crustal structure of the Eastern Alps and Bohemian Massif along longitude 13.3°E. *Tectonophysics*, *744*, 239–255. https://doi.org/10.1016/j.tecto.2018.07.001

Hinsch, R. (2013). Laterally varying structure and kinematics of the Molasse fold and thrust belt of the Central Eastern Alps: Implications for exploration. *AAPG Bulletin*, *97*(10), 1805–1831. https://doi.org/10.1306/04081312129

Hoinkes, G., Koller, F., & Rantitsch, G. (1999). *Alpine metamorphism of the Eastern Alps* [Text/html,application/pdf,text/html]. https://doi.org/10.5169/SEALS-60203

Horváth, F., Bada, G., Szafián, P., Tari, G., Ádám, A., & Cloetingh, S. (2006). Formation and deformation of the Pannonian Basin: Constraints from observational data. *Geological Society, London, Memoirs*, *32*(1), 191–206. https://doi.org/10.1144/GSL.MEM.2006.032.01.11

Hülscher, J., Fischer, G., Grunert, P., Auer, G., & Bernhardt, A. (2019). Selective Recording of Tectonic Forcings in an Oligocene/Miocene Submarine Channel System: Insights From New Age Constraints and Sediment Volumes From the Austrian Northern Alpine Foreland Basin. *Frontiers in Earth Science*, *7*, 302. https://doi.org/10.3389/feart.2019.00302

Jadoul, F., & Nicora, A. (1986). Stratigrafia e Paleogeografia Ladinico-Carnica delle Alpi Carniche Orientali (Versante Nord della Val Canale, Friuli). *Riv. It. Paleont. Strat.*, *92*(2), 201–238.

Jozi Najafabadi, A., Haberland, C., Le Breton, E., Handy, M. R., Verwater, V. F., Heit, B., Weber, M., & the AlpArray and AlpArray SWATH-D Working Groups. (2022). Constraints on Crustal Structure in the Vicinity of the Adriatic Indenter (European Alps) From *Vp* and *Vp* / *Vs* Local Earthquake Tomography. *Journal of Geophysical Research: Solid Earth*, *127*(2). https://doi.org/10.1029/2021JB023160

Karousova, H., Plomerova, J., & Babuska, V. (2013). Upper-mantle structure beneath the southern Bohemian Massif and its surroundings imaged by high-resolution tomography. *Geophysical Journal International*, *194*(2), 1203–1215. https://doi.org/10.1093/gji/ggt159

Kästle, E. D., & Paffrath, M. (2023). Advances in imaging the Alpine crust and mantle. *Abstracts of the Annual AlpArray and 4D-MB Scientific Meeting, Bad Hofgastein 2023*, 3. https://doi.org/10.17169/REFUBIUM-41043

Kästle, E. D., Rosenberg, C., Boschi, L., Bellahsen, N., Meier, T., & El-Sharkawy, A. (2020). Slab break-offs in the Alpine subduction zone. *International Journal of Earth Sciences*, *109*(2), 587–603. https://doi.org/10.1007/s00531-020-01821-z

Kennett, B. L. N., Engdahl, E. R., & Buland, R. (1995). Constraints on seismic velocities in the Earth from traveltimes. *Geophysical Journal International*, *122*(1), 108–124. https://doi.org/10.1111/j.1365-246X.1995.tb03540.x

Klotz, T., Pomella, H., Reiser, M., Fügenschuh, B., & Zattin, M. (2019). Differential uplift on the boundary between the Eastern and the Southern European Alps: Thermochronologic constraints from the Brenner Base Tunnel. *Terra Nova*, *31*(3), 281–294. https://doi.org/10.1111/ter.12398

Koulakov, I., Kaban, M. K., Tesauro, M., & Cloetingh, S. (2009). *P*—And *S* -velocity anomalies in the upper mantle beneath Europe from tomographic inversion of ISC data. *Geophysical Journal International*, *179*(1), 345–366. https://doi.org/10.1111/j.1365-246X.2009.04279.x

Kuhlemann, J., & Kempf, O. (2002). Post-Eocene evolution of the North Alpine Foreland Basin and its response to Alpine tectonics. *Sedimentary Geology*, *152*(1–2), 45–78. https://doi.org/10.1016/S0037-0738(01)00285-8

Kummerow, J., Kind, R., Oncken, O., Giese, P., Ryberg, T., Wylegalla, K., & Scherbaum, F. (2004). A natural and controlled source seismic profile through the Eastern Alps: TRANSALP. *Earth and Planetary Science Letters*, *225*(1–2), 115–129. https://doi.org/10.1016/j.epsl.2004.05.040

Kurz, W., Handler, R., & Bertoldi, C. (2008). Tracing the exhumation of the Eclogite Zone (Tauern Window, Eastern Alps) by 40Ar/39Ar dating of white mica in eclogites. *Swiss Journal of Geosciences*, *101*(S1), 191–206. https://doi.org/10.1007/s00015-008-1281-1

Kurz, W., Neubauer, F., & Genser, J. (1996). *Kinematics of Penninic nappes (Glockner Nappe and basement-cover nappes) in the Tauern Window (Eastern Alps, Austria) during subduction and Penninc-Austroalpine collision* [Text/html,application/pdf]. https://doi.org/10.5169/SEALS-167914

Laubscher, H. P. (1990). The problem of the deep structure of the Southern Alps: 3-D material balance considerations and regional consequences. *Tectonophysics*, *176*(1–2), 103–121. https://doi.org/10.1016/0040-1951(90)90261-6

Le Breton, E., Bernhardt, A., Neumeister, R., Heismann, C., Borzi, A., Hülscher, J., Sanders, R., Grunert, P., Handy, M. R., & McPhee, P. J. (2023). Early Miocene tectono-sedimentary shift in the eastern North Alpine Foreland Basin and its relation to changes in tectonic style in the Eastern Alps. *Abstracts of the Annual AlpArray and 4D-MB Scientific Meeting, Bad Hofgastein 2023*. Annual AlpArray and 4D-MB Scientific Meeting, Bad Hofgastein, Austria. https://doi.org/10.17169/REFUBIUM-41056

Linzer, H.-G., Decker, K., Peresson, H., Dell'Mour, R., & Frisch, W. (2002). Balancing lateral orogenic float of the Eastern Alps. *Tectonophysics*, *354*(3–4), 211–237. https://doi.org/10.1016/S0040-1951(02)00337-2

Lippitsch, R. (2002). *Lithosphere and upper mantle P-wave velocity structure beneath the Alps by high-resolution teleseismic tomography* [PhD Thesis, ETH Zurich]. https://doi.org/10.3929/ETHZ-A-004484684

Liu, Y., Genser, J., Handler, R., Friedl, G., & Neubauer, F. (2001). ^{40}Ar/ ^{39}Ar muscovite ages from the Penninic-Austroalpine plate boundary, Eastern Alps. *Tectonics*, *20*(4), 526–547. https://doi.org/10.1029/2001TC900011

Lüschen, E., Borrini, D., Gebrande, H., Lammerer, B., Millahn, K., Neubauer, F., & Nicolich, R. (2006). TRANSALP—deep crustal Vibroseis and explosive seismic profiling in the Eastern Alps. *Tectonophysics*, *414*(1–4), 9–38. https://doi.org/10.1016/j.tecto.2005.10.014

Lüschen, E., Lammerer, B., Gebrande, H., Millahn, K., & Nicolich, R. (2004). Orogenic structure of the Eastern Alps, Europe, from TRANSALP deep seismic reflection profiling. *Tectonophysics*, *388*(1–4), 85–102. https://doi.org/10.1016/j.tecto.2004.07.024

Luth, S. W., & Willingshofer, E. (2008). Mapping of the post-collisional cooling history of the Eastern Alps. *Swiss Journal of Geosciences*, *101*(S1), 207–223. https://doi.org/10.1007/s00015-008-1294-9

Malusà, M. G., Guillot, S., Zhao, L., Paul, A., Solarino, S., Dumont, T., Schwartz, S., Aubert, C., Baccheschi, P., Eva, E., Lu, Y., Lyu, C., Pondrelli, S., Salimbeni, S., Sun, W., & Yuan, H. (2021). The Deep Structure of the Alps Based on the CIFALPS Seismic Experiment: A Synthesis. *Geochemistry, Geophysics, Geosystems*, *22*(3), e2020GC009466. https://doi.org/10.1029/2020GC009466

Mancktelow, N. S., Stöckli, D. F., Grollimund, B., Müller, W., Fügenschuh, B., Viola, G., Seward, D., & Villa, I. M. (2001). The DAV and Periadriatic fault systems in the Eastern Alps south of the Tauern window. *International Journal of Earth Sciences*, *90*(3), 593–622. https://doi.org/10.1007/s005310000190

Maros, G., Albert, G., Szeiler, R. B., Fodor, L., Gyalog, Jocha-Edelényi, E., Kercsmár, Zs., Magyari, Á., Maigut, V., Maros, G., Nádor, A., Orosz, L., Palotás, K., Selmeczi, I., Uhrin, A., Vikor, Zs., Atzenhofer, B., Berka, R., Bottig, M., … Trajanova, M. (2012). *Summary report of the Geological Models Transenergy Project*. http:// transenergy-eu.geologie.ac.at/

Masalimova, L. U., Lowe, D. R., Mchargue, T., & Derksen, R. (2015). Interplay between an axial channel belt, slope gullies and overbank deposition in the Puchkirchen Formation in the Molasse Basin, Austria. *Sedimentology*, *62*(6), 1717–1748. https://doi.org/10.1111/sed.12201

Mellere, Stefani, & Angevine. (2000). Polyphase Tectonics through subsidence analysis: The Oligo-Miocene Venetian and Friuli Basin, north-east Italy. *Basin Research*, *12*(2), 159–182. https://doi.org/10.1046/j.1365-2117.2000.00120.x

Merlini, S., Doglioni, C., Fantoni, R., & Ponton, M. (2002). Analisi strutturale lungo un profilo geologico tra la linea Fella-Sava e l'avampaese adriatico (Friuli Venezia Giulia-Italia). *Mem. Soc. Geol. It.*, *57*, 293–300.

Mey, J., Scherler, D., Wickert, A. D., Egholm, D. L., Tesauro, M., Schildgen, T. F., & Strecker, M. R. (2016). Glacial isostatic uplift of the European Alps. *Nature Communications*, *7*(1), 13382. https://doi.org/10.1038/ncomms13382

Mitterbauer, U., Behm, M., Brückl, E., Lippitsch, R., Guterch, A., Keller, G. R., Koslovskaya, E., Rumpfhuber, E.-M., & Šumanovac, F. (2011). Shape and origin of the East-Alpine slab constrained by the ALPASS teleseismic model. *Tectonophysics*, *510*(1–2), 195–206. https://doi.org/10.1016/j.tecto.2011.07.001

Most, P. (2003). *Late Alpine Cooling Histories of Tectonic Blocks Along the Central Part of the Transalp Traverse (Inntal—Gadertal): Constraints from Geochronology*. Eberhardt-Karls-Universität Tübingen.

Moulin, A., & Benedetti, L. (2018). Fragmentation of the Adriatic Promontory: New Chronological Constraints From Neogene Shortening Rates Across the Southern Alps (NE Italy). *Tectonics*, *37*(9), 3328–3348. https://doi.org/10.1029/2018TC004958

Moulin, A., Benedetti, L., Rizza, M., Jamšek Rupnik, P., Gosar, A., Bourlès, D., Keddadouche, K., Aumaître, G., Arnold, M., Guillou, V., & Ritz, J. (2016). The Dinaric fault system: Large-scale structure, rates of slip, and Plio-Pleistocene evolution of the transpressive northeastern boundary of the Adria microplate. *Tectonics*, *35*(10), 2258–2292. https://doi.org/10.1002/2016TC004188

Mroczek, S., Tilmann, F., Pleuger, J., Yuan, X., & Heit, B. (2023). Investigating the Eastern Alpine–Dinaric transition with teleseismic receiver functions: Evidence for subducted European crust. *Earth and Planetary Science Letters*, *609*, 118096. https://doi.org/10.1016/j.epsl.2023.118096

Nussbaum, C. (2000). *Neogene Tectonics and Thermal Maturity of the Easternmost Southern Alps (Friuli Area, Italy)* [Doctoral Thesis]. Université de Neuchâtel.

Oldow, J. S., Channell, J. E. T., Catalano, R., & D'Argenio, B. (1990). Contemporaneous thrusting and large-scale rotations in the western Sicilian fold and thrust belt. *Tectonics*, *9*(4), 661–681. https://doi.org/10.1029/TC009i004p00661

Ortner, H., Aichholzer, S., Zerlauth, M., Pilser, R., & Fügenschuh, B. (2014). *Geometry, amount, and sequence of thrusting in the Subalpine Molasse of western Austria and southern Germany, European Alps*. 30.

Ortner, H., C. von Hagke, A. Sommaruga, S. Mock, J. Mosar, R. Hinsch, & A. Beidinger. (2022). The northern Deformation Front of the European Alps. In C. Rosenberg & N. Bellahsen (Eds.), *Geodynamics of the Alps 3*. ISTE-Wiley.

Ortner, H., Reiter, F., & Brandner, R. (2006). Kinematics of the Inntal shear zone–sub-Tauern ramp fault system and the interpretation of the TRANSALP seismic section, Eastern Alps, Austria. *Tectonophysics*, *414*(1–4), 241–258. https://doi.org/10.1016/j.tecto.2005.10.017

Paffrath, M., Friederich, W., Schmid, S. M., Handy, M. R., & the AlpArray and AlpArray-Swath D Working Group. (2021). Imaging structure and geometry of slabs in the greater Alpine area – a P-wave travel-time tomography using AlpArray Seismic Network data. *Solid Earth*, *12*(11), 2671–2702. https://doi.org/10.5194/se-12-2671-2021

Pfiffner, O. A. (1993). The structure of the Helvetic nappes and its relation to the mechanical stratigraphy. *Journal of Structural Geology*, *15*(3–5), 511–521. https://doi.org/10.1016/0191-8141(93)90145-Z

Picotti, V., Prosser, G., & Castellarin, A. (1995). *Structures and Kinematics of the Giudicarie-Val Trompia Fold and Thrust Belt (Central Southern Alps, Northern Italy)* (Vol. 47). University of Padova.

Picotti, V., Romano, M. A., Ponza, A., Guido, F. L., & Peruzza, L. (2022). The Montello Thrust and the Active Mountain Front of the Eastern Southern Alps (Northeast Italy). *Tectonics*, *41*(12). https://doi.org/10.1029/2022TC007522

Poli, M. E., & Zanferrari, A. (2018). *The Seismogenic Sources of the 1976 Friuli Earthquakes: A new seismotectonic model for the Friuli area*. https://doi.org/10.4430/bgta0209

Pomella, H., Flöss, D., Speckbacher, R., Tropper, P., & Fügenschuh, B. (2016). The western end of the Eoalpine High-Pressure Belt (Texel unit, South Tyrol / Italy). *Terra Nova*, *28*(1), 60–69. https://doi.org/10.1111/ter.12191

Pomella, H., Klötzli, U., Scholger, R., Stipp, M., & Fügenschuh, B. (2011). The Northern Giudicarie and the Meran-Mauls fault (Alps, Northern Italy) in the light of new paleomagnetic and geochronological data from boudinaged Eo-/Oligocene tonalites. *International Journal of Earth Sciences*, *100*(8), 1827–1850. https://doi.org/10.1007/s00531-010-0612-4

Pomella, H., Stipp, M., & Fügenschuh, B. (2012). Thermochronological record of thrusting and strike-slip faulting along the Giudicarie fault system (Alps, Northern Italy). *Tectonophysics*, *579*, 118–130. https://doi.org/10.1016/j.tecto.2012.04.015

Ponton, M. (2010). *Architettura delle Alpi Friulane*. Museo Friulano di Storia Narturale. https://arts.units.it/handle/11368/2309482?mode=complete

Ratschbacher, L., Frisch, W., Linzer, H.-G., & Merle, O. (1991). Lateral extrusion in the eastern Alps, Part 2: Structural analysis. *Tectonics*, *10*(2), 257–271. https://doi.org/10.1029/90TC02623

Reid, M. R., Schleiffarth, W. K., Cosca, M. A., Delph, J. R., Blichert-Toft, J., & Cooper, K. M. (2017). Shallow melting of MORB -like mantle under hot continental lithosphere, C entral A natolia. *Geochemistry, Geophysics, Geosystems*, *18*(5), 1866–1888. https://doi.org/10.1002/2016GC006772

Rosenberg, C. L., Berger, A., Bellahsen, N., & Bousquet, R. (2015). Relating orogen width to shortening, erosion, and exhumation during Alpine collision: ALPINE WIDTH AND COLLISIONAL SHORTENING. *Tectonics*, *34*(6), 1306–1328. https://doi.org/10.1002/2014TC003736

Rosenberg, C. L., & Kissling, E. (2013). Three-dimensional insight into Central-Alpine collision: Lower-plate or upper-plate indentation? *Geology*, *41*(12), 1219–1222. https://doi.org/10.1130/G34584.1

Rosenberg, C. L., Schneider, S., Scharf, A., Bertrand, A., Hammerschmidt, K., Rabaute, A., & Brun, J.-P. (2018). Relating collisional kinematics to exhumation processes in the Eastern Alps. *Earth-Science Reviews*, *176*, 311–344. https://doi.org/10.1016/j.earscirev.2017.10.013

Royden, L., & Burchfiel, B. C. (1989). Are systematic variations in thrust belt style related to plate boundary processes? (The western Alps versus the Carpathians). *Tectonics*, *8*(1), 51–61. https://doi.org/10.1029/TC008i001p00051

Rudmann, J., Tanner, D. C., Stipp, M., & Pomella, H. (2023, May 15). Balancing a cross-section through the western Tauern Window using non-plane strain. https://doi.org/10.5194/egusphere-egu23-15666

Scharf, A., Handy, M. R., Favaro, S., Schmid, S. M., & Bertrand, A. (2013). Modes of orogen-parallel stretching and extensional exhumation in response to microplate indentation and roll-back subduction (Tauern Window, Eastern Alps). *International Journal of Earth Sciences*, *102*(6), 1627–1654. https://doi.org/10.1007/s00531-013-0894-4

Schlunegger, F., & Castelltort, S. (2016). Immediate and delayed signal of slab breakoff in Oligo/Miocene Molasse deposits from the European Alps. *Scientific Reports*, *6*(1), 31010. https://doi.org/10.1038/srep31010

Schlunegger, F., & Kissling, E. (2022). *Slab load controls beneath the Alps on the source-to-sink sedimentary pathways in the Molasse basin* [Other]. display. https://doi.org/10.5194/egusphere-egu22-3801

Schmid, S. M., Fugenschuh, B., Kissling, E., & Schuster, R. (2004). Tectonic map and overall architecture of the Alpine orogen. *Eclogae Geologicae Helvetiae*, *97*(1), 93–117. https://doi.org/10.1007/s00015-004-1113-x

Schmid, S. M., Pfiffner, O. A., Froitzheim, N., Schönborn, G., & Kissling, E. (1996). Geophysical-geological transect and tectonic evolution of the Swiss-Italian Alps. *Tectonics*, *15*(5), 1036–1064. https://doi.org/10.1029/96TC00433

Schmid, S. M., Scharf, A., Handy, M. R., & Rosenberg, C. L. (2013). The Tauern Window (Eastern Alps, Austria): A new tectonic map, with cross-sections and a tectonometamorphic synthesis. *Swiss Journal of Geosciences*, *106*(1), 1–32. https://doi.org/10.1007/s00015-013-0123-y

Schönborn, G. (1992). Alpine Tectonics and Kinematic Models of the Central Southern Alps. *Memorie Degli Istituti Di Geologia e Mineralogia Dell'Universita Di Padova*, *XLIV*, 229–393.

Schönborn, G. (1999). Balancing cross sections with kinematic constraints: The Dolomites (northern Italy). *Tectonics*, *18*(3), 527–545. https://doi.org/10.1029/1998TC900018

Schuster, R., Kollerm, F., Hoeck, V., Hoinkes, G., & Bousquet, R. (2004). Explanatory notes to the map: Metamorphic structure of the Alps—Metamorphic evolution of the Eastern Alps. *Mitteilungen Der Österreichischen Mineralogischen Gesellschaft*, *149*, 71–95.

Selverstone, J. (1993). *Micro-to macroscale interactions between deformational and metamorphic processes, Tauern Window, Eastern Alps* [Text/html,application/pdf,text/html]. https://doi.org/10.5169/SEALS-55571

Serretti, P., & Morelli, A. (2011). Seismic rays and traveltime tomography of strongly heterogeneous mantle structure: Application to the Central Mediterranean: Traveltime tomography of mantle structure. *Geophysical Journal International*, *187*(3), 1708–1724. https://doi.org/10.1111/j.1365-246X.2011.05242.x

Sinclair, H. D. (1997). Tectonostratigraphic model for underfilled peripheral foreland basins: An Alpine perspective. *Geological Society of America Bulletin*, *109*(3), 0324. https://doi.org/10.1130/0016-7606(1997)109<0324:TMFUPF>2.3.CO;2

Spada, M., Bianchi, I., Kissling, E., Agostinetti, N. P., & Wiemer, S. (2013). Combining controlled-source seismology and receiver function information to derive 3-D Moho topography for Italy. *Geophysical Journal International*, *194*(2), 1050–1068. https://doi.org/10.1093/gji/ggt148

Sperner, B., Ratschbacher, L., & Nemčok, M. (2002). Interplay between subduction retreat and lateral extrusion: Tectonics of the Western Carpathians. *Tectonics*, *21*(6). https://doi.org/10.1029/2001TC901028

Steenken, A., Siegesmund, S., Heinrichs, T., & Fügenschuh, B. (2002). Cooling and exhumation of the Rieserferner Pluton (Eastern Alps, Italy/Austria). *International Journal of Earth Sciences*, *91*(5), 799–817. https://doi.org/10.1007/s00531-002-0260-4

Sternai, P., Sue, C., Husson, L., Serpelloni, E., Becker, T. W., Willett, S. D., Faccenna, C., Di Giulio, A., Spada, G., Jolivet, L., Valla, P., Petit, C., Nocquet, J.-M., Walpersdorf, A., & Castelltort, S. (2019). Present-day uplift of the European Alps: Evaluating mechanisms and models of their relative contributions. *Earth-Science Reviews*, *190*, 589–604. https://doi.org/10.1016/j.earscirev.2019.01.005

Stöckhert, B., Brix, M. R., Kleinschrodt, R., Hurford, A. J., & Wirth, R. (1999). Thermochronometry and microstructures of quartz—A comparison with experimental flow laws and predictions on the temperature of the brittle–plastic transition. *Journal of Structural Geology*, *21*(3), 351–369. https://doi.org/10.1016/S0191-8141(98)00114-X

Tesauro, M., Kaban, M. K., & Cloetingh, S. A. P. L. (2008). EuCRUST-07: A new reference model for the European crust. *Geophysical Research Letters*, *35*(5), 2007GL032244. https://doi.org/10.1029/2007GL032244

TRANSALP Working Group, Gebrande, H., Lüschen, E., Bopp, M., Bleibinhaus, F., Lammerer, B., Oncken, O., Stiller, M., Kummerow, J., Kind, R., Millahn, K., Grassl, H., Neubauer, F., Bertelli, L., Borrini, D., Fantoni, R., Pessina, C., Sella, M., Castellarin, A., … Bernabini, M. (2002). First deep seismic reflection images of the Eastern Alps reveal giant crustal wedges and transcrustal ramps. *Geophysical Research Letters*, *29*(10). https://doi.org/10.1029/2002GL014911

Ustaszewski, K., Schmid, S. M., Fügenschuh, B., Tischler, M., Kissling, E., & Spakman, W. (2008). A map-view restoration of the Alpine-Carpathian-Dinaridic system for the Early Miocene. *Swiss Journal of Geosciences*, *101*(S1), 273–294. https://doi.org/10.1007/s00015-008-1288-7

Van Der Meer, D. G., Van Hinsbergen, D. J. J., & Spakman, W. (2018). Atlas of the underworld: Slab remnants in the mantle, their sinking history, and a new outlook on lower mantle viscosity. *Tectonophysics*, *723*, 309–448. https://doi.org/10.1016/j.tecto.2017.10.004

Verwater, V. F., Le Breton, E., Handy, M. R., Picotti, V., Jozi Najafabadi, A., & Haberland, C. (2021). Neogene kinematics of the Giudicarie Belt and eastern Southern Alpine orogenic front (northern Italy). *Solid Earth*, *12*(6), 1309–1334. https://doi.org/10.5194/se-12-1309-2021

Viola, G., Mancktelow, N. S., & Seward, D. (2001). Late Oligocene-Neogene evolution of Europe-Adria collision: New structural and geochronological evidence from the Giudicarie fault system (Italian Eastern Alps). *Tectonics*, *20*(6), 999–1020. https://doi.org/10.1029/2001TC900021

Von Blanckenburg, F., & Davies, J. H. (1995). Slab breakoff: A model for syncollisional magmatism and tectonics in the Alps. *Tectonics*, *14*(1), 120–131. https://doi.org/10.1029/94TC02051

Wagreich, M., & Faupl, P. (1994). *Palaeogeography and geodynamic evolution of the Gosau Group of the Northern Calcareous Alps (Late Cretaceous, Eastern Alps, Austria)*. 20.

Winterer, E. L., & Bosellini, A. (1981). Subsidence and Sedimentation on Jurassic Passive Continental Margin, Southern Alps, Italy. *AAPG Bulletin*, *65*, 394–421.

Wolff, R., Hetzel, R., Dunkl, I., & Anczkiewicz, A. A. (2021). New constraints on the exhumation history of the western Tauern Window (European Alps) from thermochronology, thermokinematic modeling, and topographic analysis. *International Journal of Earth Sciences*, *110*(8), 2955–2977. https://doi.org/10.1007/s00531-021-02094-w

Wortel, M. J. R., & Spakman, W. (2000). Subduction and Slab Detachment in the Mediterranean-Carpathian Region. *Science*, *290*(5498), 1910–1917. https://doi.org/10.1126/science.290.5498.1910

Zanferrari, A., Masetti, D., Monegato, G., & Poli, M. E. (2013). *Carta Geologica d'Italia 1:50000, Sheet 49 – Gemona Del Friuli.* [Map]. ISPRA - Servizio Geologico d'Italia.

Zhu, H., Bozdağ, E., & Tromp, J. (2015). Seismic structure of the European upper mantle based on adjoint tomography. *Geophysical Journal International*, *201*(1), 18–52. https://doi.org/10.1093/gji/ggu492

Zingg, A., Handy, M. R., Hunziker, J. C., & Schmid, S. M. (1990). Tectonometamorphic history of the Ivrea Zone and its relationship to the crustal evolution of the Southern Alps. *The Nature of the Lower Continental Crust*, *182*(1), 169–192. https://doi.org/10.1016/0040-1951(90)90349-D

Manuscript submitted to Tectonics: Peer review pending.

Tectonics

Supporting Information for

Post-collisional reorganisation of the Eastern Alps in 4D: Crust and mantle structure

Peter J. McPhee[1] and Mark R. Handy[1, 2]

1. Institute of Geological Sciences, Freie Universität Berlin, Germany

2. Institute of Geological Sciences, Universität Bern, Switzerland

Contents of this file

Text S1 to S3

Introduction

This file contains details of geological maps used to construct cross-sections in the main article (Figures 6, 8, 9, 10)

S1 TRANSALP (Figures 6A and 8 of main article)

Main cross-section

Servizio Geologico d'Italia (1977). Carta Geologica d'Italia 1:50000, Sheet 28 – La Marmolada. ISPRA – Servizio Geologico d'Italia, Rome

Servizio Geologico d'Italia (2007). Carta Geologica d'Italia 1:50000, Sheet 29 – Cortina D'Ampezzo. ISPRA – Servizio Geologico d'Italia, Rome

Servizio Geologico d'Italia (2022). Carta Geologica d'Italia 1:50000, Sheet 46 – Longarone. ISPRA – Servizio Geologico d'Italia, Rome

Servizio Geologico d'Italia (1992). Carta Geologica d'Italia 1:50000, Sheet 63 – Belluno. ISPRA – Servizio Geologico d'Italia, Rome

Servizio Geologico d'Italia (1969). Carta Geologica d'Italia 1:100000, Sheet 1-4a – Passo del Brennero e Bressanone. ISPRA – Servizio Geologico d'Italia, Rome

Servizio Geologico d'Italia (1969). Carta Geologica d'Italia 1:100000, Sheet 11 – M. Marmolada. ISPRA – Servizio Geologico d'Italia, Rome

Castiglioni, B. (1931). Carta Geologica del Gruppo della Civeta, 1:25000. Memorie dell' Istituto Geologico dell R. Universita di Padova, Vol. IX.

Additional maps used in offset sections

Kreuss, O. (2007). GEOFAST 1:50000, Sheet 89 – Angath. Geologischen Bundesanstalt, Wien.

Pavlik, W. (2008). GEOFAST 1:50000, Sheet 90 – Kuftstein. Geologischen Bundesanstalt, Wien.

Kreuss, O. (2008). GEOFAST 1:50000, Sheet 120 – Wörgl. Geologischen Bundesanstalt, Wien.

Kreuss, O. (2008). GEOFAST 1:50000, Sheet 121 – Neukirchen am Großvenediger. Geologischen Bundesanstalt, Wien.

Moser., M. & Pavlik, W. (2014). GEOFAST 1:50000, Sheet 150 – Mayrhofen. Geologischen Bundesanstalt, Wien.

Karl, F. & Schmidegg, O. (1979). Geologische Karte der Republik Österreich 1:50000, Sheet 151 – Krimml. Geologischen Bundesanstalt, Wien.

Frank, W., Miller, C., Pestal, G. (1987). Geologische Karte der Republik Österreich 1:50000, Sheet 152 – Matrei in Osttirol. Geologischen Bundesanstalt, Wien.

Moser., M. (2018). GEOFAST 1:50000, Sheet 177 – Sankt Jakob in Defereggen. Geologischen Bundesanstalt, Wien.

Kreuss, O. (2018). GEOFAST 1:50000, Sheet 178 – Hopfgarten in Defereggen. Geologischen Bundesanstalt, Wien.

Linner, M., Reitner, J.M., Pavlik, W. (2013). Geologische Karte der Republik Österreich 1:50000, Sheet 179 – Lienz. Geologischen Bundesanstalt, Wien.

Schönlaub, H.P. (1997). Geologische Karte der Republik Österreich 1:50000, Sheet 196 – Obertilliach. Geologischen Bundesanstalt, Wien.

S2 EASI (Figures 6B and 9 of main article)

Main cross-section

van Husen, D. (1989). Geologische Karte der Republik Österreich 1:50000, Sheet 65 – Mondsee. Geologischen Bundesanstalt, Wien.

Plöchinger, B. (1982). Geologische Karte der Republik Österreich 1:50000, Sheet 95 – Sankt Wolfgang im Salzkammergut. Geologischen Bundesanstalt, Wien.

Neubauer, F. & Moser, M. (2022). GEOFAST 1:50000, Sheet 126 – Radstadt. Geologischen Bundesanstalt, Wien.

Häusler, H. (1995). Geologische Karte der Republik Österreich 1:50000, Sheet 156 – Muhr. Geologischen Bundesanstalt, Wien.

Pestal, G., Rataj, W., Reitner, J.M., Schuster R. (2006). Geologische Karte der Republik Österreich 1:50000, Sheet 156 – Spittal an der Drau. Geologischen Bundesanstalt, Wien.

Schönlaub, H.P. (1989). Geologische Karte der Republik Österreich 1:50000, Sheet 199 – Hermagor. Geologischen Bundesanstalt, Wien.

Battista Carulli, G., Della Vedova, B., Podda, F., Slejko, D., Zanolla, C. (2006). Carta Geologica del Friuli Venezia Giulia 1:150000. Servizio Geologico Regione Autonoma Friuli Venezia Giulia.

Zanferrari, A., Masetti, D., Monegato, G., & Poli, M. E. (2013). Carta Geologica d'Italia 1:50000, Sheet 49 – Gemona Del Friuli. ISPRA - Servizio Geologico d'Italia - Regione Autonoma Friuli Venezia Giulia.

Zanferrari, A., Avigliano, R., Monegato, G., Paiero, G., & Poli, M. E. (2008). Carta Geologica d'Italia 1:50000, Sheet 66 – Udine. APAT-Servizio Geologico d'Italia – Regione Autonoma Friuli Venezia Giulia.

Additional maps used in offset sections

Schäffer, G. (1982). Geologische Karte der Republik Österreich 1:50000, Sheet 96 – Bad Ischl. Geologischen Bundesanstalt, Wien.

Moser, M. & Pavlik, W. (2014). GEOFAST 1:50000, Sheet 98 – Liezen. Geologischen Bundesanstalt, Wien.

Mandl, G.W. & Matura, A. (1995). Geologische Karte der Republik Österreich 1:50000, Sheet 127 – Schladming. Geologischen Bundesanstalt, Wien.

Metz, K. (1979). Geologische Karte der Republik Österreich 1:50000, Sheet 129 – Donnersbach. Geologischen Bundesanstalt, Wien.

Exner, C., Hejl, E., Mandl, G.W. (2005). Geologische Karte der Republik Österreich 1:50000, Sheet 157 – Tamsweg. Geologischen Bundesanstalt, Wien.

Thurner, A. (1958). Geologische Karte der Republik Österreich 1:50000, Sheet 159 – Murau. Geologischen Bundesanstalt, Wien.

Thurner, A. & van Husen, D. (1978). Geologische Karte der Republik Österreich 1:50000, Sheet 160 – Neumarkt in Steiermark. Geologischen Bundesanstalt, Wien.

Pistonik, J. (1996). Geologische Karte der Republik Österreich 1:50000, Sheet 183 – Radenthein. Geologischen Bundesanstalt, Wien.

Thiedig, F., van Husen, D., Pistonik, J. (1999). Geologische Karte der Republik Österreich 1:50000, Sheet 186 – Sankt Veit an der Glan. Geologischen Bundesanstalt, Wien.

Anderle, N. (1977). Geologische Karte der Republik Österreich 1:50000, Sheet 200 – Arnoldstein. Geologischen Bundesanstalt, Wien.

Anderle, N. (1977). Geologische Karte der Republik Österreich 1:50000, Sheet 201-210 – Villach - Assling. Geologischen Bundesanstalt, Wien.

Kahler, F. (1962). Geologische Karte der Republik Österreich 1:50000, Sheet 203 – Umgebung von Klagenfurt. Geologischen Bundesanstalt, Wien.

S3 EW (Figures 6C and 10 of main article)

Maps in addition to those listed above for TRANSALP and EASI

Exner, C., Hejl, E., Mandl, G.W. (2005). Geologische Karte der Republik Österreich 1:50000, Sheet 157 – Tamsweg. Geologischen Bundesanstalt, Wien.

Küpper, H. (1958). Geologische Karte der Republik Österreich 1:50000, Sheet 158 & 158 – Stadl and Murau. Geologischen Bundesanstalt, Wien.

Thurner, A., van Husen, D. (1978). Geologische Karte der Republik Österreich 1:50000, Sheet 160 – Steiermark. Geologischen Bundesanstalt, Wien.

Moser, M. (2015). GEOFAST 1:50000, Sheet 161 – Knittelfeld. Geologischen Bundesanstalt, Wien.

Becker, L.P. (1979). Geologische Karte der Republik Österreich 1:50000, Sheet 162 – Köflach. Geologischen Bundesanstalt, Wien.

Ebner, F., Becker, L.P., Schuster, R. (2017). Geologische Karte der Republik Österreich 1:50000, Sheet 163 – Voitsberg. Geologischen Bundesanstalt, Wien.

Flügel, H.W., Nowotny, A., Gross, M. (2011). Geologische Karte der Republik Österreich 1:50000, Sheet 164 – Graz. Geologischen Bundesanstalt, Wien.